NOVEL HIGH REFRACTIVE INDEX, THERMALLY CONDUCTIVE ADDITIVES FOR HIGH BRIGHTNESS WHITE LEDS

By

Richard Stephen Hutchison

A Thesis Submitted to the Graduate
Faculty of Rensselaer Polytechnic Institute
in Partial Fulfillment of the
Requirements for the degree of

MASTER OF SCIENCE

Major Subject: Materials Science and Engineering

Approved by the
Examining Committee:

Dr. Linda Schadler, Thesis Adviser

Dr. Rahmi Ozisik, Member

Dr. Chaitanya Ullal, Member

Rensselaer Polytechnic Institute
Troy, New York

June, 2015
(For Graduation August 2015)

© Copyright 2015
by
Richard Stephen Hutchison
All Rights Reserved

CONTENTS

LIST OF TABLES

LIST OF FIGURES

ACKNOWLEDGMENTS

Greater minds have come before and laid the way for my progression through this project. I can say without a doubt that if it weren't for my peers across campus and the country, the faculty and staff at Rensselaer, and my family, I would not have made it this far. None of what I did was a solo effort, but the byproduct of inspiration from those around me. As I know I will many more times in the future, I must express my gratitude to Gina and Adrian for being solid pillars of support, encouragement, and inspiration. Without you by my side, I would not have pushed so hard and succeeded to come this far.

I owe all of what I achieved to my parents, Jim and Diane, for giving me the second chance to turn my life around. Love and patience from you carried me through some of the most trying periods as I transitioned from degenerate to driven. Listening patiently when I needed someone to bounce an idea off of or to ramble on to and providing me with your wisdom and experience when I encountered new obstacles are just two of the countless ways you aided me on this journey. You raised me and I gave you hell for the first twenty years of my life, so now I aspire to continually surprise (hopefully pleasantly) and honor you with my constant striving to be a better leader, friend, and servant to those around me.

Owed to my academic family, is a great debt of gratitude; first to Prof. Linda Schadler, for her profound patience, direct guidance, and unwillingness to give up on me through some of the rougher times I have had. Under her guidance I was able to learn and grow as both an academic and a person over the course of this project.

Müteşekkirim Rahmi sana her sey icin. As both my undergraduate advisor and graduate coadvisor, Prof. Rahmi Ozisik capably communicated with me, got into my head and helped me stay on track, and looked out for me when I may not have thought to do so for myself.

Rivaling the hours I spent on campus, Prof. Chaitanya Ullal has kept himself productive and busy while still making time to give me feedback on my writing and suggestions on my work, for this I owe him a great many thanks.

Research at Rensselaer would have been nigh impossible without the help of a great many people. Your help and guidance did not go unnoticed.

Multitudes of thanks go out to Dr. Bob Karlicek for your patience and good humor while describing ideas to me; my peers: Ying, Peng, Emily, Alex, Tim, Hafez, Indira, Irene, Casey, and Yanhui for being good friends and excellent minds to spar with; my colleagues Collin Hitchcock, Casey Goodwin, Deniz Rende, Don VanSteele, Joel Morgan, Rob Planty, Ray Dove and Scott McCallum for discussing various ideas and helping me solve tricky problems; Dr. Theo Borca-Tasciuc for allowing me to use his equipment and lab space; and last, but most importantly: Nancy Beatty, Lauretta Carroll, Barbara Jordan, Dana Chichester, Lori Robichaud, Meeli Leith, and Amy Edmans, all of you were good humored, friendly, and helped keep me perky through the rougher days, you were my mothers away from home and I am so glad to have shared this experience with you!

Everyone mentioned, and those not mentioned, thank you, for where would I be without you (especially Ainsley for helping me keep my grammar and wordiness in check)**?**

ABSTRACT

In prior works the inclusion of nanoparticle fillers has typically been shown to increase the thermal conductivity or refractive index of polymer nanocomposites separately. High refractive index zirconia nanoparticles have already proved their merit in increasing the optical efficiency of encapsulated light emitting diodes. However, the thermal properties of zirconia-silicone nanocomposites have yet to be investigated. While phosphor-converted light emitting diodes are at the forefront of solid-state lighting technologies for producing white light, they are plagued by efficiency losses due to excessive heating at the semiconductor die and in and around the phosphor particles, as well as photon scattering losses in the phosphor layer. It would then be of great interest if the high refractive index nanoparticles were found to both be capable of increasing the refractive index, thus reducing the optical scattering, and also the thermal conductivity, channeling more heat away from the LED die and phosphors, mitigating efficiency losses from heat.

Thermal conductance measurements on unfilled and nanoparticle loaded silicone samples were conducted to quantify the effect of the zirconia nanoparticle loading on silicone nanocomposite thermal conductivity. An increase in thermal conductivity from 0.27 W/mK to 0.49 W/mK from base silicone to silicone with 33.5 wt% zirconia nanoparticles was observed. This trend closely mirrored a basic rule of mixtures prediction, implying a further enhancement in thermal conductivity could be achieved at higher nanoparticle loadings.

The optical properties of transparency and light extraction efficiency of these composites were also investigated. While overall the zirconia nanocomposite showed good transparency, there was a slight decrease at the shorter wavelengths with increasing zirconia content. For longer wavelength LEDs, such as green or red, this might not matter, but phosphor-converted white LEDs use a blue LED as the photon source making this decrease in transparency important to note. This decrease in transparency may be partially or wholly why a decrease in light extraction efficiency is observed at the 33.5 wt% zirconia loading fraction used for the LED samples.

Preliminary aging studies under full and enhanced power conditions were conducted over 500 and 1000 hours to observe any changes in the spectral output power and phosphor conversion efficiency of the LEDs due to inclusion of the zirconia nanoparticles. It was found that the nanoparticles have no negative effect on the aging properties but also show no enhancement in relative output power over a preliminary aging study. However, their inclusion did result in increased phosphor conversion efficiency over the use of an unfilled silicone. This increase was seen as around a 10% or greater enhancement for the nanocomposite over that for the base Sylgard silicone.

These experiments were originally conducted on the commercially available methylated Sylgard 184 silicone and then again on a higher refractive index methyl-phenyl silicone from Momentive. While some of the results from the Momentive silicone were perplexing, it was seen that, even without the inclusion of nanoparticles, the Momentive silicone had a higher refractive index, better aging properties, and a higher phosphor conversion efficiency over 500 hours under enhanced power conditions, warranting further studies into methyl-phenyl silicone nanocomposites.

1. Introduction

The study and application of nano-scale fillers for light emitting diode (LED)-based applications is an emerging field. Improvements in the light extraction efficiency (LEE) of LED encapsulant materials through the use of high refractive index titania (TiO_2) and zirconia (ZrO_2) nanoparticles have already been demonstrated.[1–3] This finding holds great potential because a bare, unencapsulated semiconductor suffers from light lost to significant internal reflection resulting from the high refractive index (RI) mismatch between the semiconductor and air.[1]

The advancement of white-light solid state lighting (SSL) devices is of great interest in order to replace current, less efficient incandescent and florescent ones. Currently, the common commercial way to make high-brightness white LEDs is to combine a LED with a color converting phosphor of a complimentary color to that emitted by the LED. While this is a convenient way to make white-light SSL units, light scattering in the phosphors and heating from both the LED die and the phosphors lead to less efficient LED units. Since the effects of nanoparticle (NP) fillers on the efficiency of phosphor-converted LEDs (pcLEDs) have not been widely investigated and the potential benefits to efficiency, energy, and cost are significant, further investigation into the applicability of these high RI fillers is warranted.

Polymer nanocomposites for SSL applications were developed and studied for this project. The goal of the work is to show that the inclusion of nanoparticles improves the thermal and optical properties, and thus efficiency, of silicone-encapsulated pcLEDs.

1.1 Background

Between 2012 and 2013 the number of LED based lighting applications in the U.S. increased by more than double, to approximately 105 million SSL units resulting in an annual energy cost savings of $1.8 billion in 2013 alone (again more than double that from 2012).[4] SSL takes the lead in lighting technologies, replacing inefficient incandescent, fluorescent (including compact fluorescent lamps (CFLs)), and other units due to its potential efficiency, color rendering, and unit lifetime, with lifetimes exceeding even the best linear fluorescent systems that boast up to 25,000 hours.[5,6] The vast leap in unit lifetime from incandescent to LEDs can be seen in Table 1.1.

Table 1.1. Comparison of lighting technologies.[4] Below the luminous efficacy, correlated color temperature (CCT), and 70% lumen depreciation, defined as the useful lifetime of a lighting source before its output decreases below 70%, denoted L_{70}, metrics are reported.

Product Type	Luminous Efficacy (lm/W)	CCT (K)	L_{70} (hours)
LED PAR38 Lamp	78	3000	50000
LED Troffer 2' x 4'	131	3000	75000
LED High/Low-Bay Fixture	119	3500	75000
Linear Fluorescent System[7]	108	4100	25000
CFL	73	2700	12000
Halogen	20	2750	8400
Incandescent	15	2760	1000

1.1.1 Replacing the Old Standard, Ways to Make White Light

The reason incandescent-based lighting is still favored as a lighting source is that it more adequately mimics the broad spectrum of natural sunlight. However, incandescent bulbs achieve this by turning electrical energy supplied into heat, some of which is radiated in the visible spectrum, while the majority is radiated in the infrared. So, while this process yields a spectrum that resembles natural sunlight, it comes at the cost of lost efficiency.

To overcome these inefficiencies, companies and government entities, such as the United States Department of Energy (DOE), have established roadmaps and assertive programs to lead the way in bringing SSL closer to mimicking natural light, with the DOE's SSL program goals including a 50% system efficiency for LEDs that "accurately [reproduce] sunlight spectrum."[4] Several different methods of creating white light using SSL have been developed to lead the way in replacing the old paradigm.

White light LEDs can be created using di-, tri-, or tetrachromatic sources that involve the mixing of complimentary colors typically made of blue and yellow, for the dichromatic source, blue green, and red for the trichromatic source, and blue, cyan, green, and red for the tetrachromatic sources.[5] These source colors can be produced by having multiple LED dies, each with a specific color, by using organic florescent dye molecules with an LED source, or by having a combination of a semiconductor source and color-converting inorganic phosphors.[5,7,8]

The current commercial way to make white emitting LEDs is to combine a blue LED with a down-converting phosphor, such as YAG:Ce, which converts some of the incident blue light into a yellow emission which subsequently mixes with the remainder transmitted blue to yield white, see Figure 1.1.[9] Typical ways to construct a pcLED include mixing the phosphor into the silicone to create a slurry as an encapsulant, placing the phosphor remotely away from the semiconductor die, or applying them conformally to the die in a thin, form-fitting layer, see Figure 1.2.[10]

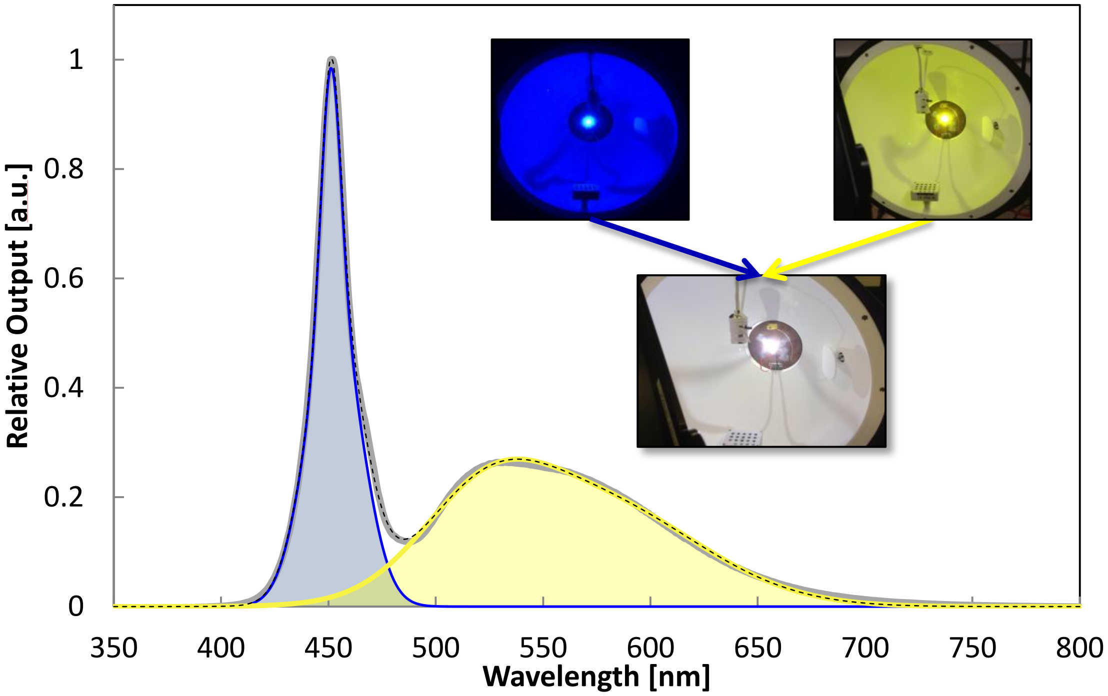

Figure 1.1. Radiometric spectrum of pcLED using YAG:Ce phosphor. Data from phosphor coated Royal Blue LED sample with plain silicone encapsulant dome.

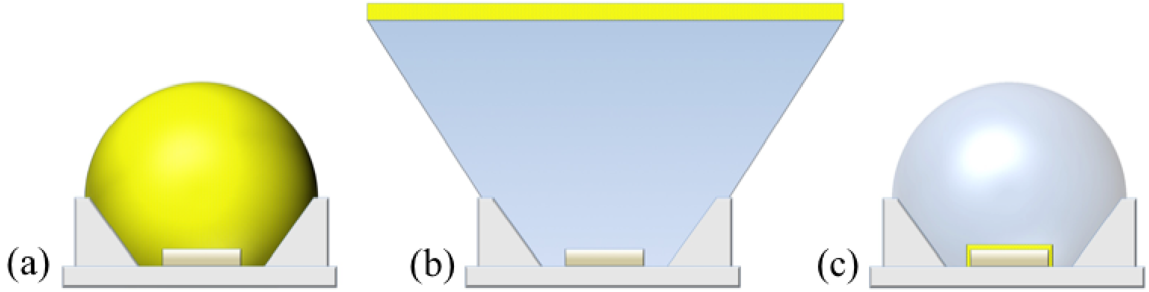

Figure 1.2. Possible phosphor placements for pcLEDs: From left to right: (a) phosphor slurry (b) remote phosphor placement (c) encapsulated conformal coating. Yellow in the graphic indicates phosphor in encapsulant material while blue represents plain encapsulant regions.

While other advanced architectures have been designed, such as the scattered photon extraction (SPE) or the enhanced light extraction by internal reflection (ELiXIR) pcLED, depicted in Figure 1.3, these novel configurations are based on one of the aforementioned constructions.[10,11]

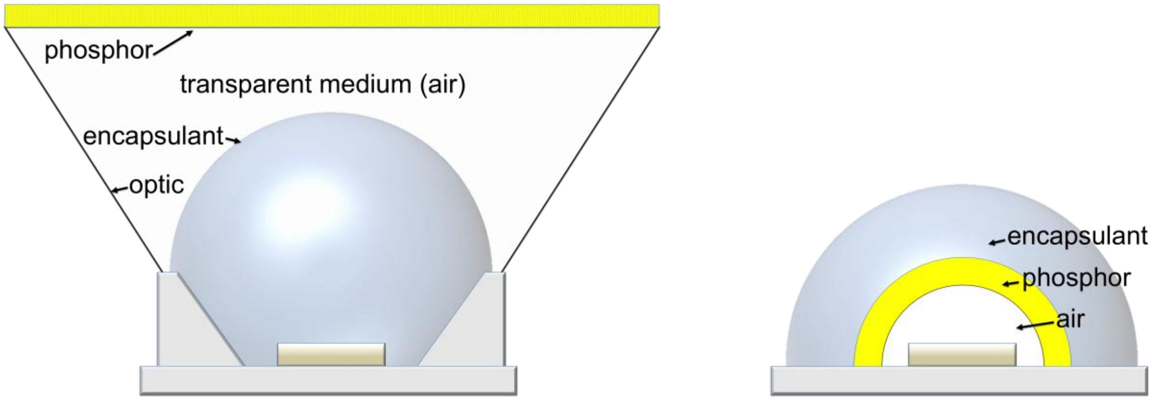

Figure 1.3. Advanced phosphor placement architectures. From left to right are the SPE and ELiXIR pcLED setups, recreated from Ref.10 and Ref.11.[10,11]

The SPE and ELiXIR setups are based on the remote phosphor placement scheme as it has been shown to reduce light lost to backscattering and subsequent internal reflection as well as increase the phosphor conversion efficiency and thermal management properties. However, the phosphor must be located at a distance from the LED die, which, along with the extra packaging required to make these advanced architectures, results in an overall larger LED unit and more difficult manufacturing.[10,12] On the other hand, the conformal coating scheme adds negligible thickness to the final product, requires a minimal amount of phosphor (as it only needs to cover the photon emitting portion of the diode), and is already common place in industry.

While a conformal coating of phosphor on blue LEDs is a convenient and compact solution for creating white-light, there are still issues that need to be addressed prior to pcLEDs realizing their full potential.

1.1.2 Issues with pcLEDs

1.1.2.1 Fresnel Reflection Losses Due to RI Mismatch

A well-known issue with LED units is the reduced light escape cone due to Fresnel reflection losses resulting from the RI mismatch between the semiconductor die and air. This has been overcome by introducing encapsulant materials with RI between that of the semiconductor and air. A more ingenious innovation of this idea came about with the graded-refractive index (GRIN) encapsulant scheme, in which the layer closest to the semiconductor has the highest RI, nearly matching that of the semiconductor, with subsequent layers having decreasing RI until the final layer matches closely to air.[13,14]

However, for the case of the simple conformal coating and encapsulation, the refractive index mismatches between the LED die and conformal coating, conformal coating and encapsulant, and encapsulant and air are all potential locations for light to be lost to internal reflection, see Figure 1.4.

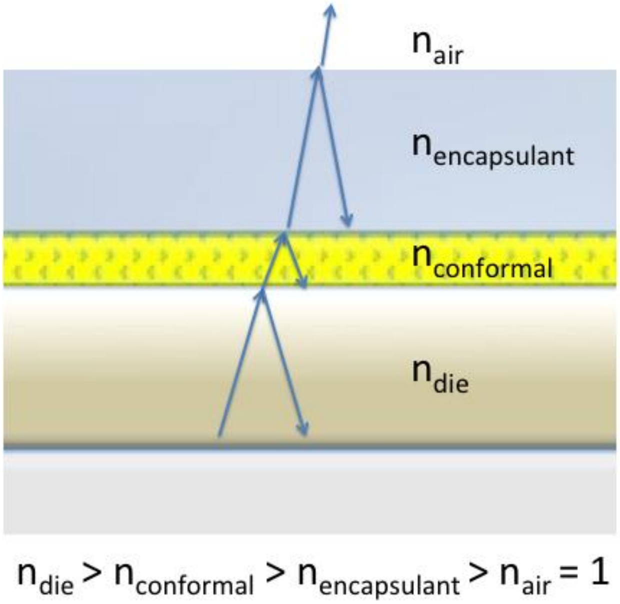

Figure 1.4. Cross-section of encapsulated and conformally coated LED showing Fresnel reflections due to differing refractive indices. The amount of light reflected at each layer is directly related to the magnitude of the refractive index mismatch between layers.

1.1.2.2 Light Lost to Scattering in Phosphors

To further aggravate the issue of light lost back into the LED, some of the photons emitted from the phosphor particles will be emitted back towards the semiconductor die or at an angle that will experience internal reflection and thus not necessarily escape the unit.[5] This, along with scattering of the light due to the phosphor particles, constitutes a second area for improvement in conformally coated pcLEDs.

1.1.2.3 Decrease in Phosphor Conversion Efficiency with Increase in Temperature

While LED efficiency is lost mainly by optical means, scattering and internal reflection, the temperature also plays a role in the efficiency of the LED and the phosphor.[15–17] Regardless of the location of the phosphor, whether conformal or remotely placed, there are Stokes shift losses during the down conversion process from blue to the lower energy yellow spectrum, see Figure 1.5a. This energy is lost in the form of non-radiative decay, which, instead transfers energy away by means of phonons.[16–18] Unfortunately, since the phosphors used in pcLED applications are typically mixed with a binder, such as silicone (which would also be used as the encapsulant material), the low thermal conductivity of the binder and encapsulant prevent these phonons from being channeled away efficiently, resulting in localized heating in the phosphor layer. Heating from the semiconductor die will also contribute to the temperature in the phosphor layer, leading to the phosphors being hotter than the LED die itself.

In either case of the conformal coating or remote placement, the phosphor experiences an increase in temperature, which has been shown to lead to a decrease in its quantum conversion efficiency as shown in Figure 1.5b.[15] This process is known as thermal quenching.[16,17] Thus, the relatively low thermal conductivity of the binder and encapsulant material leads to thermal quenching in the phosphors as the heat generated by the phosphors isn't conducted away efficiently and they experience a reduction in quantum conversion efficiency.

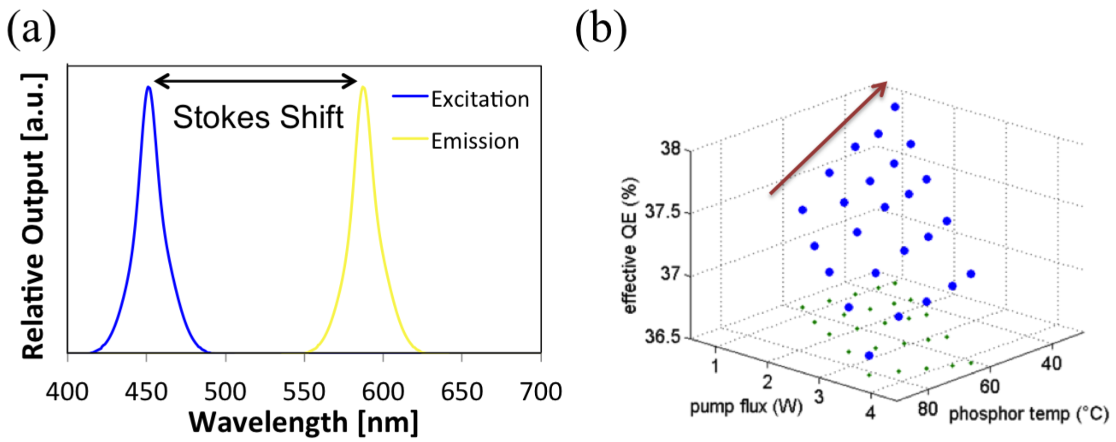

Figure 1.5. (a) Stokes shift losses and phosphor quantum efficiency. (b) The phosphor quantum conversion efficiency increases with decreasing temperature. [15]

Thus, it would be advantageous if a solution could be developed to mitigate the issues of backscattering and internal reflection, channeling more light out of the LED, phosphor, and encapsulant material, as well as channeling more heat away from the phosphors, thus cooling them down and increasing their quantum conversion efficiency. Such a solution in conjunction with a compact conformal coating would lead to smaller, easier to manufacture, and more efficient SSL units being realized.

1.1.3 Nanocomposite Solutions

Previously, Mont *et al.*[1] with monomodal grafted titania (TiO_2) NPs (average TiO_2 diameter – 40 nm) and then Li and Tao with bimodally grafted TiO_2 and zirconia (ZrO_2) (average TiO_2 and ZrO_2 radius 2.7 nm and 1.9 nm , respectively) have shown that the inclusion of these high refractive index NPs to epoxy and silicone yields an increased RI of the composite material, in turn resulting in an increased light extraction efficiency without significant loss to transmitted light.[1–3,19] The key to such improvements lies in the particle size of ~5 nm being significantly smaller than the wavelength of light, for which Rayleigh scattering is the dominant scattering mechanism.[1] The transmitted intensity (T) as a function of particle size can be modeled for Rayleigh scattering with the following equation[2,3,20]:

$$T = \frac{I}{I_0} = exp\left(-\left[\frac{32\phi_p x\pi^4 r^3 n_m^4}{\lambda^4}\left[\frac{\left(\frac{n_p}{n_m}\right)^2 - 1}{\left(\frac{n_p}{n_m}\right)^2 + 2}\right]^2\right]\right) x100\% \qquad (1.1)$$

where I and I_0 are the final and initial intensities, respectively; ϕ_p is the volume fraction of nanoparticles, x is the optical path length or the thickness of the sample in nanometers; r is the nanoparticle radius in nanometers; n_m and n_p are the refractive indices of the matrix material and nanoparticle, respectively; and λ is the wavelength of light in nanometers.[20] According to Eq. 1.1, 90% of optical transmittance could be preserved for nanoparticles sized less than or equal to 10 nm (at 10% loading (by volume), with an optical path length of 100 μm, wavelength of 450 nm, and matrix and nanoparticle refractive indices of 1.4 and 2.2, respectively); see Figure 1.6. Thus it is of great importance that the proposed particles be smaller than 10 nm in order to avoid significant losses in transmittance due to scattering phenomena.

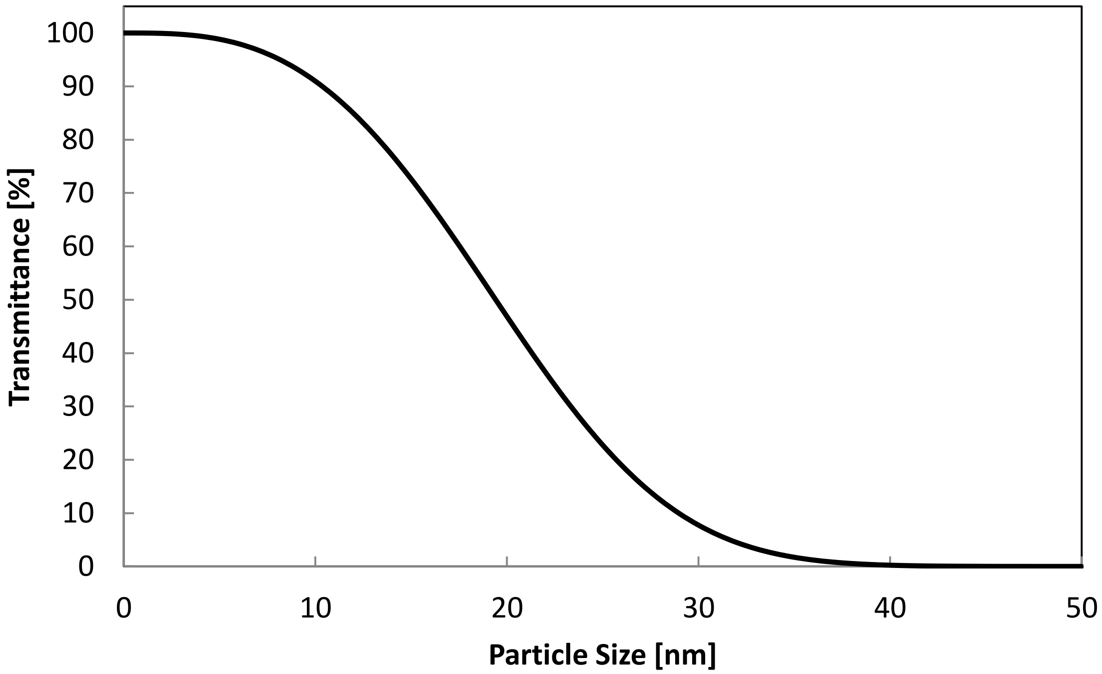

Figure 1.6. Rayleigh scattering transmittance as a function of particle size. ~90% transmittance preserved for nanoparticles sized $\leq$ 10nm.

Prior research on transparent nanocomposites with enhanced thermal conductivity has been conducted. One of the largest enhancements in thermal conductivity of a potentially viable nanocomposite for optical applications was seen in cellulose nanofiber-epoxy composites, where a 28% increase in thermal conductivity, from 0.18 W/mK to 0.23 W/mK was observed while still maintaining 80% transparency at up to 58 weight percent cellulose nanofibers.[21] Similarly, with silicone having a thermal conductivity of 0.27 W/mK and ZrO_2 with a typical thermal conductivity between 2.0 W/mK and 3.3 W/mK there is great potential for improving the nanocomposites thermal conductivity while maintaining high transparency.[22,23]

1.2 Goals and Objectives

It has previously been shown that a high refractive index, optically transparent nanocomposite can be fabricated using bimodally functionalized ZrO_2 NPs utilizing a short polymer brush to hold the NP cores apart, preventing agglomeration of the particles, and a longer brush to entangle with the matrix, thus permitting good dispersion properties of the nanoparticles, details in Figure 1.7.[2,3]

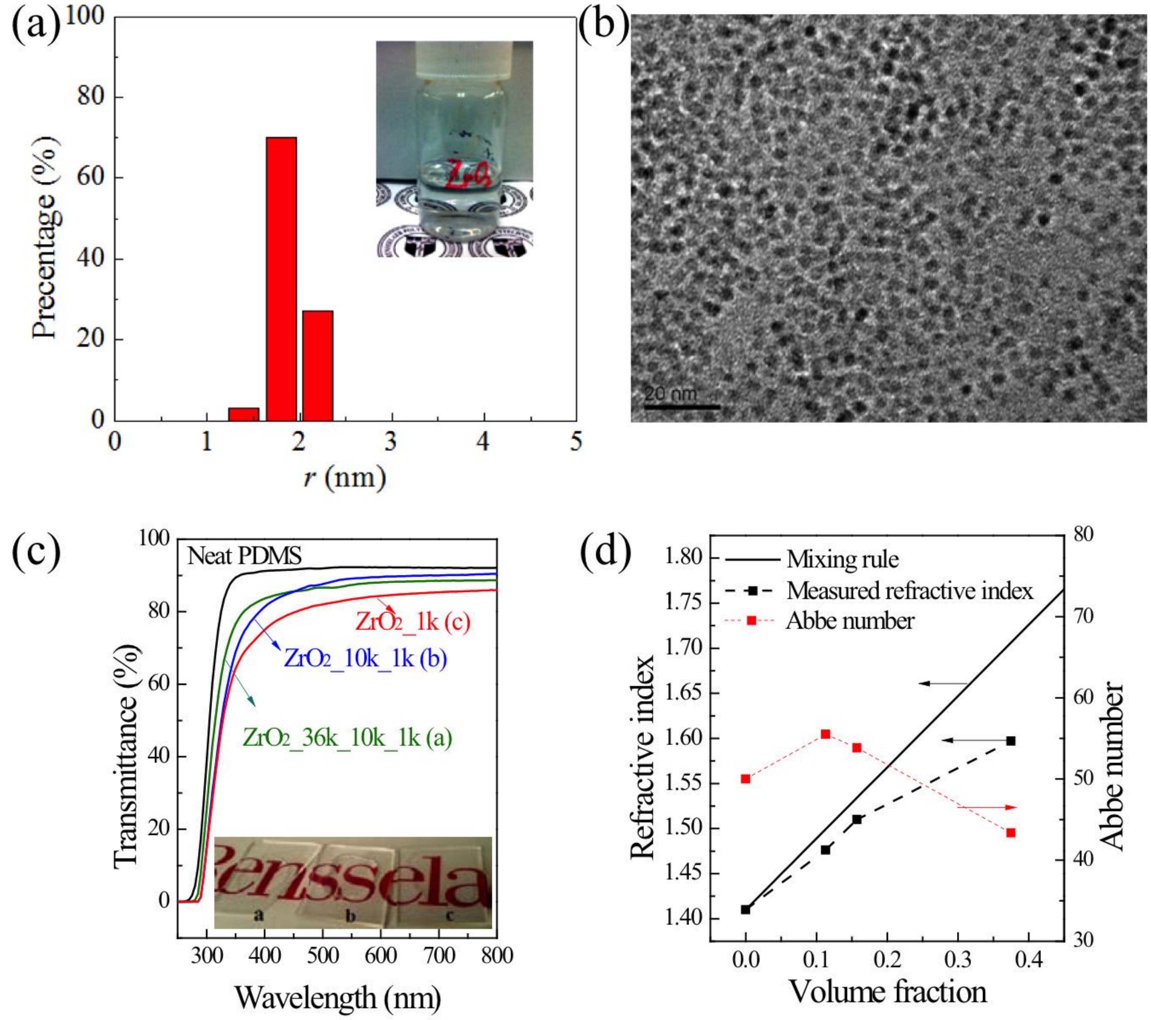

Figure 1.7. Prior work on ZrO_2 nanoparticles. (a) Particle size distribution. (b) TEM of ZrO_2 nanoparticles displaying excellent dispersion properties. (c) UV-vis transparency curves of mono-, bi-, and tri-modally functionalized ZrO_2 nanoparticles with PDMS brushes. (d) Refractive index enhancement with increasing nanoparticle loading.[3]

These well dispersed nanoparticles will be used in conjunction with a conformal coating of phosphor to attempt to increase the efficiency of pcLEDs. Thus the goal for this study is to demonstrate that the zirconia nanocomposite with phosphor can achieve a 10% or greater enhancement in phosphor conversion efficiency over that for plain silicone. This goal will be achieved through the following action items:

1.2.1 Nanoparticle Synthesis and Functionalization

In order to achieve an optically transparent, high refractive index composite material, the first target is to achieve the synthesis of ZrO_2 NPs, with a diameter of ~5 nm and a refractive index of ~2.2, through a non-aqueous solvo-thermal method and then subsequent modification of those particles with a bimodal distribution of both a short 1k and a longer 10k polydimethylsiloxane (PDMS) brushes. The grafted nanoparticles will be mixed into commercially available silicone matrix materials with a goal of achieving an index of refraction of 1.6 or greater.

1.2.2 Enhancement of Encapsulant and Phosphor Binder Properties

Composite samples will be fabricated in conformations appropriate to measure the thermal conductivity, transparency, and refractive index of the materials as a function of composite composition, with a thermal conductivity performance goal of 1 W/mK. This high refractive index, higher thermal conductivity matrix will be mixed with phosphor particles as a binder to make phosphor/zirconia/silicone conformal coatings for white-light LEDs.

1.2.3 Conformal LED Coatings

The phosphor/zirconia/silicone conformal coating will be applied to blue LEDs and the efficiency will be measured through the light extraction efficiency and phosphor quantum conversion efficiency and compared to samples prepared with plain silicone as the encapsulant and binder. The LEDs will be subjected to a 500 hour preliminary aging study under full power conditions and the spectral output and phosphor conversion efficiency will be tracked with time.

1.2.4 Higher Refractive Index Polymer System

A higher refractive index phenylated silicone brush and matrix system from Momentive will be explored in order to potentially further enhance the thermal and optical properties of the nanocomposite encapsulant material. The composite will be synthesized, characterized, and compared to the initial high refractive index methylated silicone samples.

2. Materials and Experimental Methods

2.1 Materials

For the non-aqueous, surfactant-free synthesis of zirconia (ZrO_2) nanoparticles, zirconium(IV) isopropoxide isopropanol complex (zirconia precursor) and benzyl alcohol (BA) were purchased from Sigma-Aldrich Co. LLC.

In order to functionalize the ZrO_2 nanoparticles (NPs) for dispersion, monocarboxydecyl terminated polydimethylsiloxane (MCR-B12, Mw = 1,000 g/mol) (1k PDMS) and monocarbinol terminated polydimethylsiloxane (MCR-C22, Mw = 10,000 g/mol) (10k Methyl) were purchased from Gelest Inc., and suitable hydroxyl-terminated dimethyl/diphenylpolysiloxane (MP) brushes were obtained from Momentive Performance Materials Inc. (Mw = 10,000 g/mol) (10k MP). To convert the hydroxyl-terminated PDMS (10k Methyl and 10k MP) into phosphate-terminated PDMS (P-10k Methyl and P-10k MP), phosphorus (V) oxychloride ($POCl_3$) and triethylamine (Et_3N) were purchased from Sigma-Aldrich.

Since the commercial applicability of the proposed technology is important, the well-studied commercially available Sylgard 184 ® silicone (Sylgard) (Dow Corning Corporation) was chosen as the encapsulant matrix material for the initial high refractive index system. It should be noted that the Sylgard silicone is a methylated silicone polymer with 30-60 wt% silica nanoparticles as a filler.[24] The higher refractive index, methyl/phenyl silicone system matrix was provided by Momentive in the form of vinyl-terminated PDMS. In order to crosslink the Momentive MP matrix, methylhydrosiloxane-dimethylsiloxane copolymer, trimethylsiloxane terminated (HMS-301) (Gelest) and platinum(0)-1,3-divinyl-1,1,3,3-tetramethyldisiloxane complex solution 0.05 M in poly(dimethylsiloxane), vinyl terminated solution (Sigma-Aldrich) were obtained for use as the crosslinking agent and catalyst, respectively.

Blue (B) (PR2N-3LBE-SD) and Royal Blue (RB) (PR2N-3LDE-SD) LEDs provided by ProLight Opto Technology Corporation and YAG:Ce phosphors from Dow Chemical Co. and OSRAM Gmbh, hereinafter referred to as Dow and Osram, were obtained in order to fabricate the phosphor-converted LEDs (pcLEDs).

2.2 Polymer Brush Synthesis

The 10k Methyl and 10k MP hydroxyl-terminated PDMS were taken and modified by replacing the –OH end group with a phosphate end group via a single step modification technique.[25] For this reaction 10 grams of either 10k brush was taken and dissolved in 60 mL of tetrahydrofuran (THF) in a 500 mL round bottom flask. The solution was cooled via an ice bath to 0 °C under stirring. Initially Et_3N was added dropwise and allowed to cool and then $POCl_3$ was added dropwise, in a molar ratio of 1:5:5 PDMS:Et_3N:$POCl_3$. The reaction was allowed to warm to ambient temperature as the ice melted. After 2 days the reaction was terminated using ~70 mL of DI water until the pH of the solution was below 2. The modified PDMS brushes (P-10k Methyl and P-10k MP) were extracted using CH_2Cl_2 and then separated such that the PDMS-containing organic phase was obtained and subsequently filtered over Na_2SO_4 to remove any residual water. The resulting solution was condensed using a rotary evaporator until the CH_2Cl_2 was removed. Evidence of the successful phosphate modification can be seen by the phosphate monoester peak at ~0 ppm in Figure 2.1 as well as through indirect means via thermogravimetric analysis and NP dispersion as described in later sections.

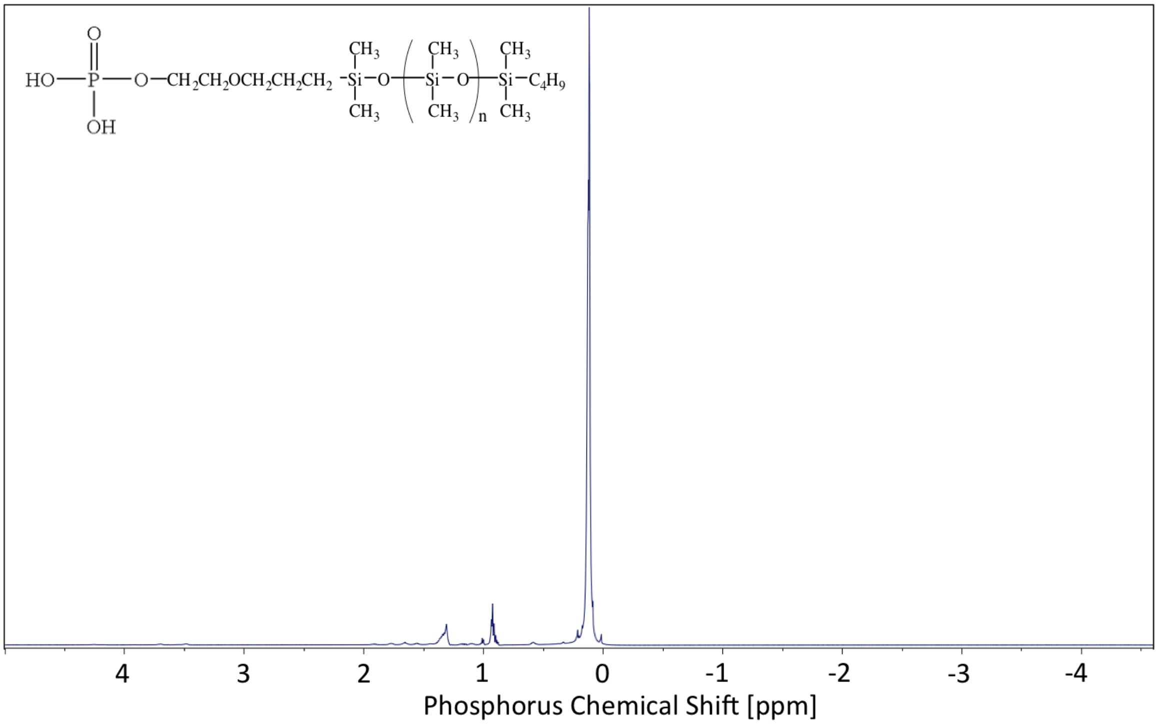

Figure 2.1. NMR spectra of P-10k Methyl PDMS showing evidence of phosphate modification via the phosphate monoester peak at ~0 ppm.[25]

2.3 Nanoparticle Synthesis

In order to synthesize the spherical zirconia nanoparticles sized ~5 nm, the zirconia precursor was added to BA in a ratio of 2.22 g precursor to 30 mL BA in a 450 mL pressure vessel (Parr Instruments).[26] The reaction was run at 240 °C for 48 hours. The resulting nanoparticles were centrifuged at 10,000 rpm for 10 minutes and the white zirconia nanoparticle precipitate was redispersed in chloroform ($CHCl_3$).

2.3.1 Functionalization

The ZrO_2 NPs in $CHCl_3$ were sonicated with carboxylic acid terminated 1k PDMS (MCR-B12) in a weight ratio of 1:0.6, PDMS:ZrO_2, to attach these short brushes to the ZrO_2 in order to shield the ZrO_2 cores from attraction and agglomeration.[3] The functionalized particles were then washed by precipitation in methanol, centrifuged at 10,000 rpm for 10 minutes, and then redispersed in $CHCl_3$. The concentration of ZrO_2 NP cores in solution and the weight ratio of ZrO_2 to ZrO_2 + 1k PDMS were determined by thermogravimetric analysis (TGA). The NPs were further functionalized by addition of the P-10k PDMS, either the methylated or MP P-10k PDMS depending on the sample, into the NP solution in a weight ratio of 2:1, 10k PDMS:ZrO_2, and then refluxing at 70°C for 24 hours. The resulting bimodally grafted nanoparticles were washed again and redispersed in $CHCl_3$ and the ZrO_2 NP core concentration and ratio of ZrO_2 to ZrO_2+1k+10k PDMS were determined by TGA. The success of grafting was also confirmed by FTIR.

2.4 Nanocomposite Fabrication

Both the NPs with methylated brushes and MP brushes were mixed in with their respective matrix material by using solvent mixing under stirring in $CHCl_3$. The Sylgard system was mixed in with the prescribed matrix to curing agent ratio of 10:1 while the Momentive matrix was cured using a ratio of 10g of matrix to 1.532 g of HMS-301 and 120 ppm of platinum catalyst. Once the mixture was homogenous the solvent was removed under vacuum to prevent discoloration and bubbles. For all samples, the nanocomposite was cured at 160 °C for a minimum of 1 hour.

2.4.1 Composite Curing

Sylgard thermal conductivity samples were molded for 24 hours in epoxy molds with cylindrical holes of diameter 6.20mm with heights 1, 2, 3, 4, 5, and 6 mm using a mirror-finish aluminum backing adhered to the molds using the same silicone composite composition as for the particular set of samples. The silicone was also taken and applied to optically transparent glass slides in a uniform 0.5 mm layer and cured on a leveled plate for 1 hour. Ellipsometry samples were made by dissolving the silicone and nanocomposite in $CHCl_3$ and spin-coating it on Si wafers at 7000 rpm for 30 seconds to produce samples with a silicone or silicone-nanocomposite thickness between 20 and 80 nm. Lastly, LED domes were fabricated by pipetting the silicone into machined a PTFE mold and cured for 1 hour. These steps were repeated to create nanocomposite samples with 10, 20, and 33.5 wt% ZrO_2 loading for both the methylated Sylgard and Momentive MP systems.

2.4.2 Determination of Phosphor Required for White Light

In order to achieve white light close to the CIE standard white point (0.33, 0.33), the volume percent (vol%) of phosphor in silicone and silicone-nanocomposite needed to be determined.[27] Since the weight percent was more convenient to work and communicate with it is reported herein, the volume percent is also included in text and in the figures. The Dow and then Osram YAG:Ce phosphors were mixed into plain Sylgard silicone in 5, 10, 15, and 65 wt% of phosphor in silicone, dissolved in $CHCl_3$, agitated to make the solution homogenous, and then immediately a drop was pipetted onto the preheated semiconductor die. It was found that dissolving the YAG-silicone composite in $CHCl_3$ with a concentration of 1 g composite to 3 mL solvent provided a solution which yielded a well-mixed conformal coating. While the thickness of the conformal coating was not known, it was thin enough to make the semiconductor features visible while still completely coating the LED die. Blue (B) LEDs and then Royal Blue (RB) LEDs were explored in conjunction with the Dow and Osram phosphors for creating white light.

2.4.3 Conformal Coating

Once the volume fraction of YAG required to achieve white light was determined, conformal coatings of YAG with the plain silicones as well as with ZrO_2 loaded samples were made for both the Sylgard and Momentive systems. The same silicone or silicone nanocomposite sample used to fabricate a set of domes was used as the binder for the phosphor in the conformal coating layer.

2.5 Characterization/ Testing

2.5.1 Dynamic Light Scattering – Zirconia NP Size

In order to determine the size of the nanoparticles, ZrO_2+1k PDMS dispersed in $CHCl_3$ was pipetted into a quartz cuvette for dynamic light scattering (DLS) testing (Brookhaven 90Plus Particle Size Analyzer). A number average plot was used to determine the particle diameter range.

2.5.2 FTIR – Polymer Brush Grafting

Fourier transform infrared (FTIR) spectroscopy was used to confirm the successful grafting of the 1k- and 10k-PDMS brushes. Samples of the as-synthesized ZrO_2 NPs, ZrO_2+1k PDMS, and ZrO_2+1k+10k PDMS were dispersed in in $CHCl_3$ and pipetted onto ZnSe plates that were placed in a liquid-sample cell. The samples were scanned from 4000 - 0 cm^{-1} to obtain the transmittance data.

2.5.3 TGA – ZrO_2 Concentration and Graft Density

After both grafting steps, the concentration of ZrO_2 NP cores in solution and the weight loss of polymer brushes were determined using thermogravimetric analysis (TGA) (TA Instruments TGA-Q50). Nanoparticles dispersed in $CHCl_3$ were pipetted into a TGA crucible in 2-100 μL amounts for a total of 200 μL for each run. The temperature was ramped from ambient temperature to 120 °C at a heating rate of 10 °C/min, held isothermally for 20 minutes to volatilize the solvent, then ramped to 800 °C at a rate of 20 °C/min and held isothermally for 10 minutes to ensure complete burn off of polymer brushes. The final mass was recorded as ZrO_2 cores and residual ash from the polymer, which was subsequently factored out in later graft density calculations.

2.5.4 Thermal Conductivity

The thermal conductivity was determined by conducting a steady-state one-dimensional thermal conduction experiment as outlined by ASTM standard D5470 and Yavari et al.[28,29] Cylindrical samples of the base Sylgard and ZrO_2 loaded Sylgard of 10, 20, and 33.5 wt% compositions were measured, see Figure 2.2a. Each sample was placed between indium plates with embedded thermocouples to measure the temperature difference across the sample. A heating element was sandwiched between the upper indium plate and an insulating block of PTFE to provide a source of temperature gradient across the sample, see Figure 2.2b.

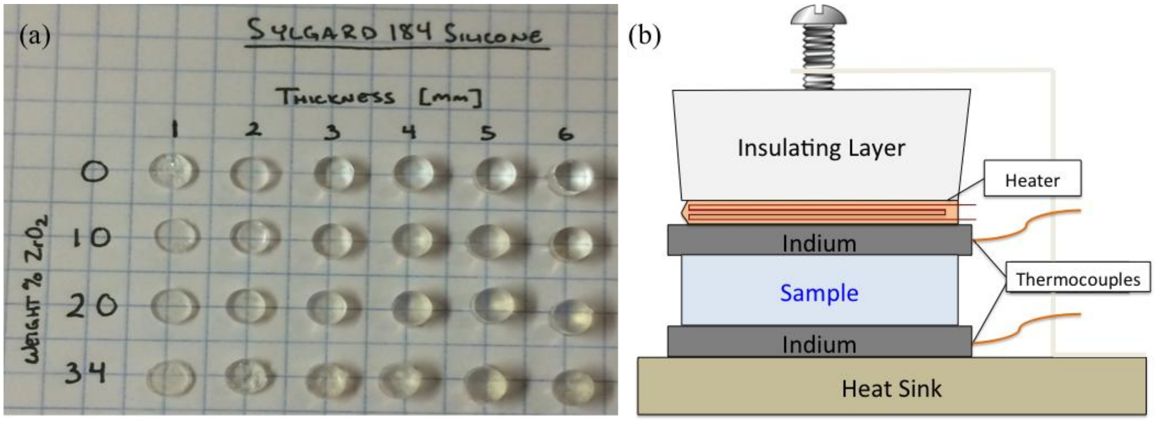

Figure 2.2. Thermal conductivity samples and setup. (a) Sylgard silicone samples from 1–6 mm height and 0–34 wt% (33.5 wt%) ZrO_2 loading. (b) Graphic illustrating the steady-state thermal conductance testing setup.

The heat loss in the setup was calibrated using a set of base Sylgard samples with a measured thermal conductivity of 0.27 W/mK, matching the literature value from Dow Corning.[22] The temperature difference across the samples and heating power applied were measured using a custom thermal conductivity setup and LabVIEW program supplied by Dr.Theodorian Borca-Tasciuc.

2.5.5 UV-Vis – Transparency

The transparency of the base Sylgard and Momentive silicones and the 10, 20, and 33.5 wt% ZrO_2 loaded samples was determined by curing the composite on glass slides, having negligible absorption in the visible range (350-800 nm), in a thickness of 0.5 mm and analyzing them from 1000-250 nm in 1 nm increments using a UV/vis spectrophotometer (Perkin-Elmer Lambda 950 UV/vis/NIR spectrophotometer).

2.5.6 Ellipsometry – Refractive Index

The refractive index of the silicone and nanocomposite was determined by using a variable angle spectroscopic ellipsometer (VASE, J.A. Woollam Co., Inc., Lincoln, NE) measuring through a range of six angles (65, 67, 69, 71, 73, 75°), and then fitting the results to a Cauchy model with a mean square error (MSE) of less than 6 for all samples except the 33.5 wt% Sylgard, which had an average MSE of 19.[3,30]

2.5.7 Integrating Sphere – Spectral Output Power

The spectral output power of the LED samples was determined using an integrating sphere (Orb-Optronix TEC-100, Labsphere CDS 1100 system). The spectral output was initially measured for the bare LEDs and then again after encapsulation with silicone, silicone-ZrO_2, silicone-YAG, or silicone-ZrO_2-YAG for both the Sylgard and Momentive systems. The spectral output of the samples was measured as a function of wavelength. Each LED had thermal grease applied to the backing and was affixed to a thermal plate which operated with a 10 °C set point in order to avoid any aging during prolonged test periods as well as to match prior testing conditions for the ZrO_2-silicone nanocomposite system. The LEDs were tested using the recommended maximum operating conditions of 350 mA and 4 V with the radiant flux measurement mode set to take a single measurement with an integration time of 370 ms averaged over 10 measurements.[31]

The spectral output power was used to assess the light extraction efficiency of the silicones and nanocomposites, and to track the aging properties and determine the phosphor quantum conversion efficiency (PCE) of the LEDs using a spectral peak deconvolution script written by O'Haver.[32]

2.5.7.1 MATLAB – Peak Deconvolution

It is important to detail exactly how the peak deconvolution and integration was conducted for future comparisons, especially since the royal blue spectrum is not like other LEDs due to its predominant peak at 450-451 nm (indigo) and shoulder around 460 nm (blue) while typical LEDs can be fitted by a single Gaussian curve.

Using the signal processing MATLAB functions from O'Haver, the peak deconvolution was achieved by determining fitting parameters to obtain a fit with error of less than 1% (typically ~0.5%) for each pcLED output spectrum at each aging data point, see Figure 2.3 for an example output. The royal blue and phosphorescence spectra were best approximated as the sum of 2 Gaussian functions each, as seen by the green curves. The spectral output power as a function of wavelength as measured from the integrating sphere can be reproduced using the following equations:

$$P_i(\lambda) = h_i * exp\left(-\left(\frac{\lambda - x_i}{0.6005612 * w_i}\right)^2\right) \qquad (2.1)$$

$$P_{total}(\lambda) = P_{RB1}(\lambda) + P_{RB2}(\lambda) + P_{P1}(\lambda) + P_{P2}(\lambda) \qquad (2.2)$$

where λ is the wavelength and h_i , x_i , w_i , are the peak height, position, and width, $P_i(\lambda)$ is the Gaussian function for an output power spectrum as a function of wavelength for which RB1, RB2, P1, and P2 represent the two distinct royal blue and phosphorescence peaks, and $P_{total}(\lambda)$ represents the total output spectrum for the LED, respectively. Integrating these spectra provided the output power of the royal blue and phosphorescence parts of the white spectrum, which were then taken and compared against the output of the initial, unmodified LED spectrum to find the PCE[33]:

$$PCE = \frac{\int P_{P1}(\lambda) + P_{P2}(\lambda) d\lambda}{\int P_{RB_o}(\lambda) d\lambda - \int P_{RB1}(\lambda) + P_{RB2}(\lambda) d\lambda} = \frac{P_P}{P_{RB_o} - P_{RB_f}} \qquad (2.3)$$

where P_P, P_{RB_o}, and P_{RB_f} are the total power of the phosphorescence, the initial royal blue spectrum of the unmodified LED, and the final royal blue portion of the converted spectrum, respectively. The PCE was tracked as a function of aging along with the relative output power as described in Section 2.5.7. It should be noted that the assignment of $P_{RB1}(\lambda)$ and $P_{RB2}(\lambda)$, as well as their phosphorescence counterparts, is somewhat arbitrary since they are summed prior to integration and are only used to recreate the royal blue or phosphorescence portion of the LED spectrum.

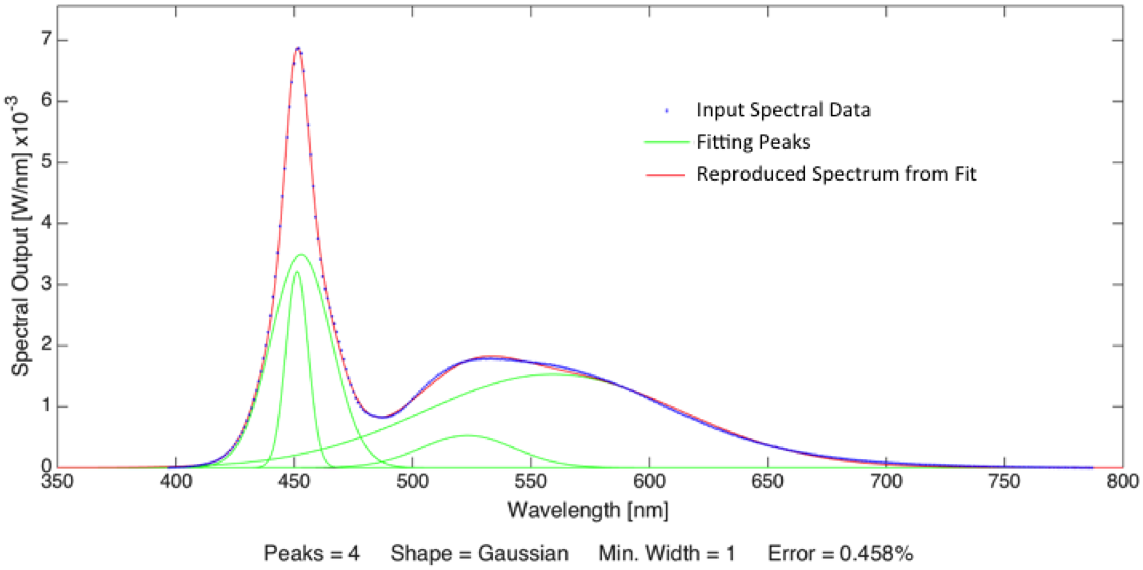

Figure 2.3. MATLAB peak deconvolution using T.C. O'Haver's peakfit script. Best fit peakfit function code: peakfit([Wavelength RB25_1022], 600, 500, 4, 1, 100, [450, 60, 460, 10, 525, 60, 550, 60]) where the function works as follows: peakfit(signal_data, center, window, number_of_peaks, peak_shape, iterations, [seed_data]). The signal_data is a matrix with x values in column 1 and y values in column 2, center is the peak center, window is the width measured from center to fit, number_of_peaks is the number of peaks used in the model, peak_shape = 1 for Gaussian, iterations = 100, the smallest number that yielded the lowest error, seed_data= [peak_wavelength, width] with entries corresponding to the guess for each peak wavelength and width to start the initial fitting. Values used were found to work well with 100 iterations.

2.5.7.2 LED Binning

Before the provided LEDs were used they had to be tested, or “binned”, to remove any variation in experimental conditions arising from differing peak wavelength and output power. The LEDs were tested, prior to modification, and sorted by output power and then dominant wavelength into bins having output power and wavelength within +/-10% and 2 nm, respectively.

2.5.8 LED Aging

To assess the aging properties of the LED samples and their applied conformal coating and encapsulant, the LEDs were affixed to heat sinks connected to temperature probes, connected in series to create a circuit for powering the LEDs, and aged by operating them continuously under full and enhanced power conditions as outlined in Table 2.1, also see Figure 2.4. Since the aging properties under what would be typical commercial operating conditions were of interest, no heating or cooling was applied to the LEDs and, instead, they were allowed to heat up from room temperature to operating temperature (~35 °C for 0.35 A and ~55 °C for 1.5 A). Due to the very minor decrease in output power over 1000 hours seen in Aging Set 1 for both maximum recommended operating current (0.35 A) and enhanced operating current (1 A), the current for Aging Set 2 was further increased in hopes of assessing any early-stage aging issues with the samples.

Table 2.1. LED preliminary aging study conditions.

Set	Time [hr]	Current [A]
Set 1 – Sylgard	0 – 609	0.35
Set 1 – Sylgard	609 – 1022	1.0
Set 2 – Momentive	0 – 497	1.5

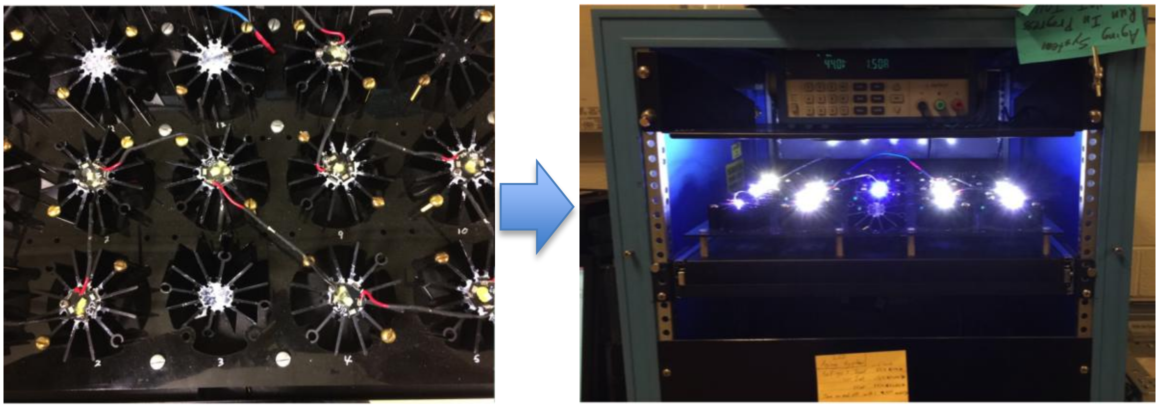

Figure 2.4. Aging setup. (left) LEDs mounted on heat sinks and connected in series for testing. (right) Aging test running in controlled environment for testing.

3. Results

3.1 Introduction

Prior to LED encapsulation, the properties of the silicones and nanocomposites used in this study were determined through a series of experiments. The nanoparticle size was assessed using DLS to determine whether the particles were near the expected size of ~5 nm. The ZrO_2 concentration in solution, weight loss due to polymer decomposition, and ZrO_2 weight ratio were determined using TGA. The success of grafting can also be seen through TGA from the two elbows in the data. Once successful ZrO_2 functionalization was determined, nanocomposite samples were made. The thermal conductivity of the silicone and then NP loaded silicone was tested as a function of weight percent loading of ZrO_2 NPs using a one-dimensional steady-state thermal conduction experiment. Since along with the thermal properties, the optical properties of the material are key to this solution, the transparency and refractive index of the samples were determined using UV-vis spectroscopy and ellipsometry, respectively. In order to achieve white light from the blue and royal blue LEDs used, the volume percent phosphor required to yield white light was determined and assessed using an integrating sphere. The sphere was also used to track the optical output of the LEDs as they were aged. Lastly, a peak fitting scrip in MATLAB was used in order to deconvolute the white spectrum into respective blue and phosphorescence spectra to determine the PCE.

3.2 Nanoparticle Synthesis and Functionalization

3.2.1 Zirconia Particle Size – DLS

The average size (diameter) of the nanoparticles (ZrO_2+1k PDMS) was investigated using DLS and found to be <10 nm (between 4 and 5 nm with a spread from 3-10 nm), see Figure 3.1.

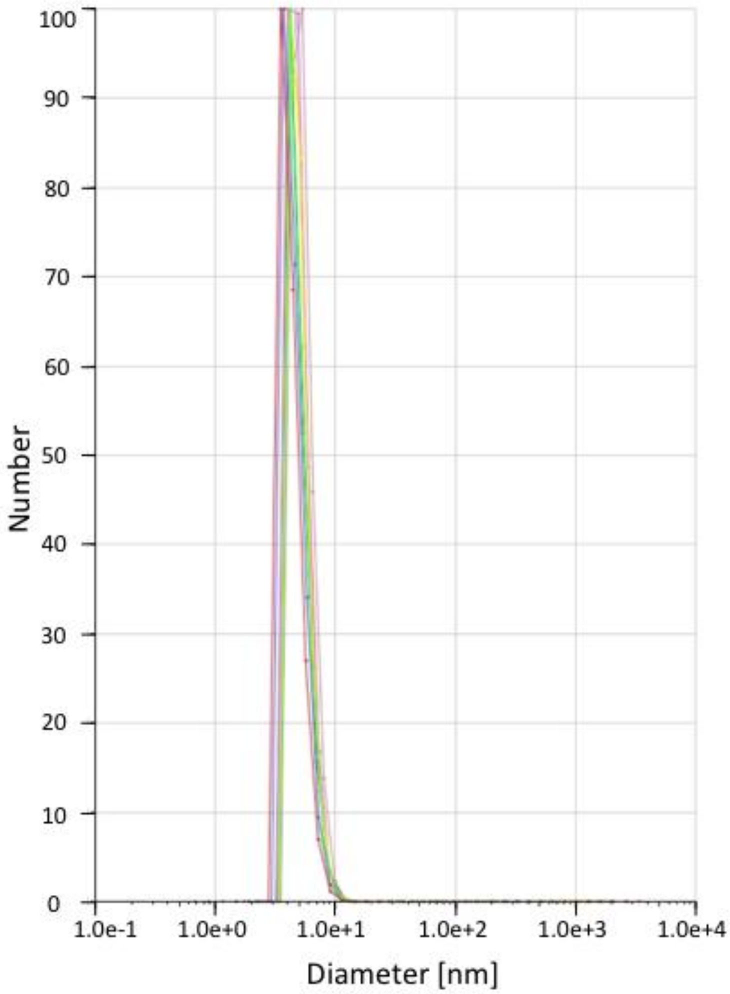

Figure 3.1. DLS of ZrO_2 NPs with 1k PDMS brushes on surface showing a predominant particle diameter of ~5 nm.

3.2.2 Polymer Brush Grafting – FTIR

The absorbance data for the as-synthesized ZrO_2 NPs shown in Figure 3.2 shows a broad band about 3350 cm^{-1} that is indicative of the surface –OH groups left over from the ZrO_2 synthesis.[34] This band disappears while bands at ~1220 and 770 cm^{-1} and the double band between 1130 and 1000 cm^{-1} appear, which are indicative of the PDMS groups Si-CH_3 and Si-O-Si, respectively. Since free-floating excess PDMS was washed away after grafting, disappearance and subsequent appearance mentioned confirm successful replacement of the surface –OH groups by the PDMS brushes.[3,34–36]

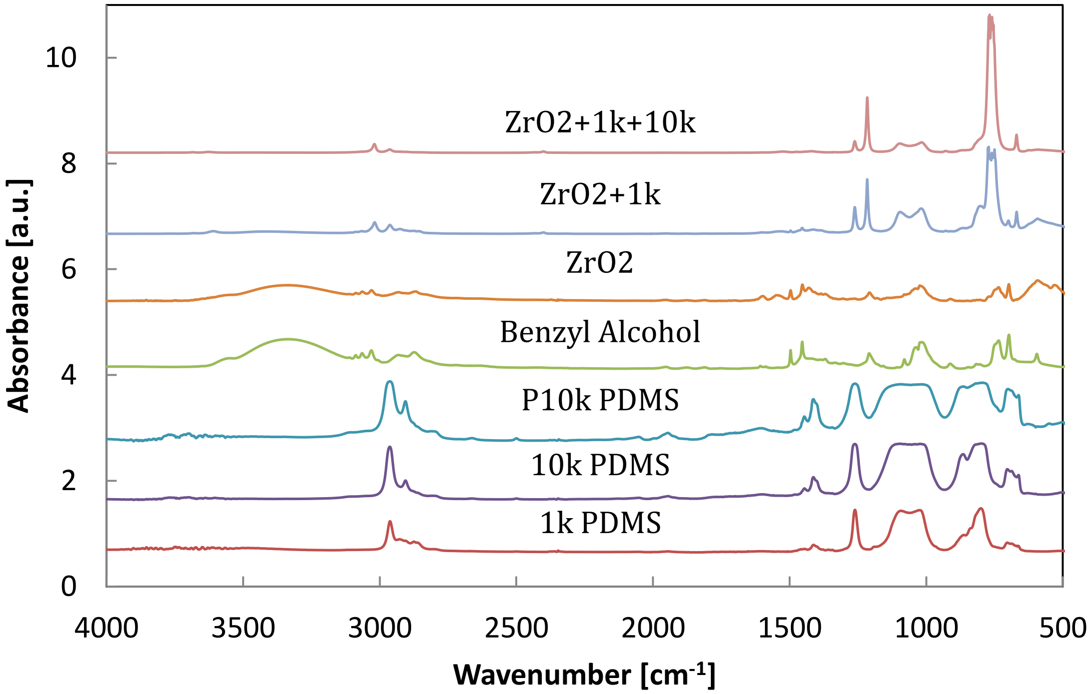

Figure 3.2. FTIR spectra of ZrO_2 NPs bare (as-synthesized), modified with 1k PDMS, and with 1k and 10k Methyl PDMS.

3.2.3 Zirconia Concentration and Grafting – TGA

TGA was used to determine the ZrO_2 concentration in solution as well as the weight loss due to 1k or 1k and 10k PDMS brushes burning up, which was used to determine the graft density. In Figure 3.3a an elbow at ~350°C for the ZrO_2+1k Methyl is indicative of the 1k PDMS brushes burning off while for the ZrO_2+1k+10k Methyl curve shows a second elbow at ~540°C which accounts for the P-10k PDMS burning off. The higher temperature for the removal of the P-10k PDMS brushes is due to the relative strength of the bond between the carboxyalkyl-terminated 1k PDMS and ZrO_2 NP and the phosphate-terminated 10k PDMS and the ZrO_2 NP, with the latter being stronger.[3] The final plateau represents the mass of zirconia NP cores in the initial 200 μL of solution and PDMS ash, and was used to determine the concentration of ZrO_2 in a given sample for use in subsequent experiment steps. The ratio of the final plateau to the initial plateau for the bimodally grafted NPs (ZrO_2+1k+10k Methyl or ZrO_2+1k+10k MP) is used to determine the maximum composite loading achievable for a given sample. In the case of Figure 3.3a this ratio is 0.37, meaning a maximum ZrO_2 core loading achievable with this sample would be 37%. In the case of the MP sample, Figure 3.3b, the grafting ratio (ZrO_2:ZrO_2+1k+10k MP) was ~0.61, potentially meaning a higher loading of ZrO_2 in silicone could be achieved. Over the various sets of samples typical grafting ratios for the methylated system were between 0.30 and 0.40 and for the phenylated system they were ~0.50 to 0.65. The curves in Figure 3.3 for the ZrO_2+1k and ZrO_2+1k+10k do not have the ash subtracted out which explains why the curve for the ZrO_2+1k+10k MP sample has a higher final weight percent than its corresponding ZrO_2+1k curve, due to the MP brushes leaving a greater weight percent ash than the 1k or 10k Methyl.

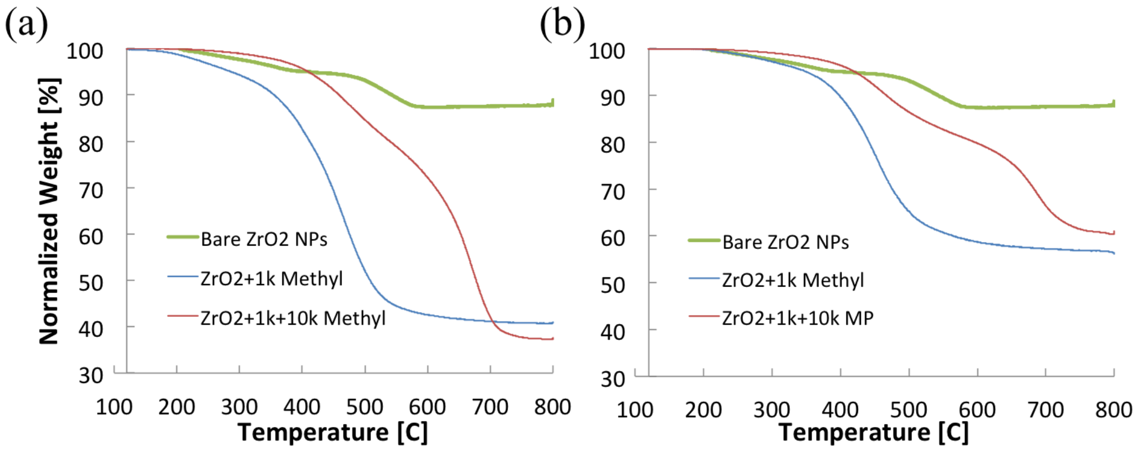

Figure 3.3. TGA curves of ZrO_2+1k+10k. (a) Sylgard system (methyl silicone). (b) Momentive system (methyl/phenyl silicone).

The TGA data can also be used to determine the graft density of the 1k or 1k and 10k PDMS. To do this, the amount of ash left behind by 1k or 10k PDMS brushes was determined by running samples of just the polymer brushes. It was determined that the 1k and 10k PDMS brushes leave about 5 wt% ash while the 10k MP brushes leave 13 wt% residue. Along with ash, residual benzyl alcohol has to be factored out of the weight of the sample. The weight fraction residual benzyl alcohol was determined in a similar manner as the PDMS ash except with the as-synthesized ZrO_2 nanoparticles after washing and being redispersed in $CHCl_3$. Once the PDMS ash and residual benzyl alcohol are factored out, the weight fraction of ZrO_2 cores and the weight loss due to 1k PDMS, and 10k PDMS can be determined and used to calculate an estimate of the PDMS graft density, σ, using[38]:

$$\sigma = r\rho z N_a * 10^{-21}/[3(1-z)\ M_n] \tag{3.1}$$

where r is the radius of the nanoparticles in nanometers, ρ is the density of zirconia in grams per centimeter cubed, z is the weight loss of organic matter (1k or 10k PDMS brushes), N_a is Avogadro's number to represent the number of brushes per mole, and M_n is the molecular weight of the PDMS being investigated. The graft density of 1k, 10k, and 10k MP PDMS can be seen in Table 3.1. In the case of the bimodally grafted samples, an effective graft density can be determined as the sum of the individual grafting densities of 1k and 10k PDMS.

Table 3.1. Graft density of PDMS on ZrO_2 NPs. Graft density for the original, methylated PDMS system and the new methyl/phenyl PDMS system and corresponding effective grafting densities (br = brushes).

	$\boldsymbol{\sigma_{1k}}$ $[\mathbf{br/nm^2}]$	$\boldsymbol{\sigma_{10k}}$ $[\mathbf{br/nm^2}]$	$\boldsymbol{\sigma_{eff}}$ $[\mathbf{br/nm^2}]$
ZrO_2+1k+10k	0.24	0.11	0.36
ZrO_2+1k+10k MP	0.19	0.02	0.21

3.3 High Refractive Index and Thermal Conductivity Composites

While a composite is an ideal way to get a desired set of properties, typically there is a tradeoff. For example, in cement, aggregates can be added to enhance the compressive strength yet if they are added in too large of a quantity it can lead to a crumbly mixture. Similarly, in the case of the ZrO_2-silicone composites, the NPs are added to increase the refractive index and, theoretically, the thermal conductivity. However, due to the brushes on the NPs surface, there is a threshold loading that can be achieved beyond which there is no room left for the matrix material. As this threshold value is approached it becomes more difficult to achieve the same hard, solid consistency that the plain, unmodified silicone has. Instead, the nanocomposite acts more like a soft rubber or gel with increased loading when crosslinked. This tradeoff is an issue since softer domes are more difficult to work with. In order to overcome this deficiency, as well as achieve high loadings of ZrO_2 cores in a nanocomposite encapsulant, readily-crosslinkable, matrix free ZrO_2-PDMS composites have been designed in prior studies.[3]

3.3.1 Thermal Conductivity Measurements

The Sylgard composite showed a near doubling in thermal conductivity from 0.27 W/mK to 0.49 W/mK from the base silicone to a 33.5 wt% (8 vol%) ZrO_2 loading. Figure 3.4.

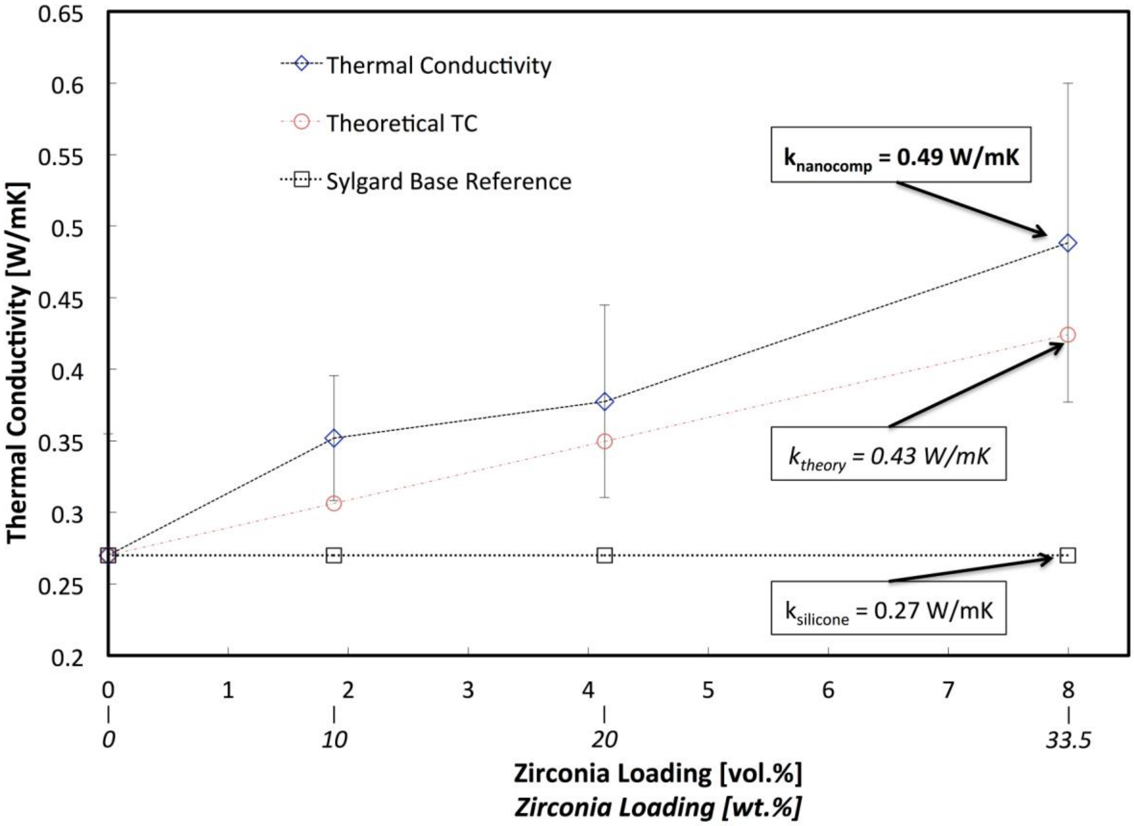

Figure 3.4. Thermal conductivity of ZrO_2 nanocomposite as a function of composite composition. The black line represents the base silicone thermal conductivity while the red is the rule of mixtures.

3.3.2 Transparency – UV-Vis

Before the nanocomposite can be used as an encapsulant material it must be determined whether or not sufficient transparency has been achieved with the material.

UV-vis measurements were used to verify that the composite transmits 85-92% in the visible spectrum, Figure 3.5. The relatively wavelength-insensitive transparency for most of the visible spectrum can be attributed to a reduction in scattering losses due to the well dispersed, highly transparent nanoparticles.[3] Both the plain Sylgard and Momentive silicones show high transparency (≥90%) across the spectrum. However, while all three of the Sylgard-ZrO_2 samples: 10, 20, and 33.5 wt%, had overlapping transparency curves, the Momentive-ZrO_2 samples showed a noticeable decrease in transparency with increasing ZrO_2 loading.

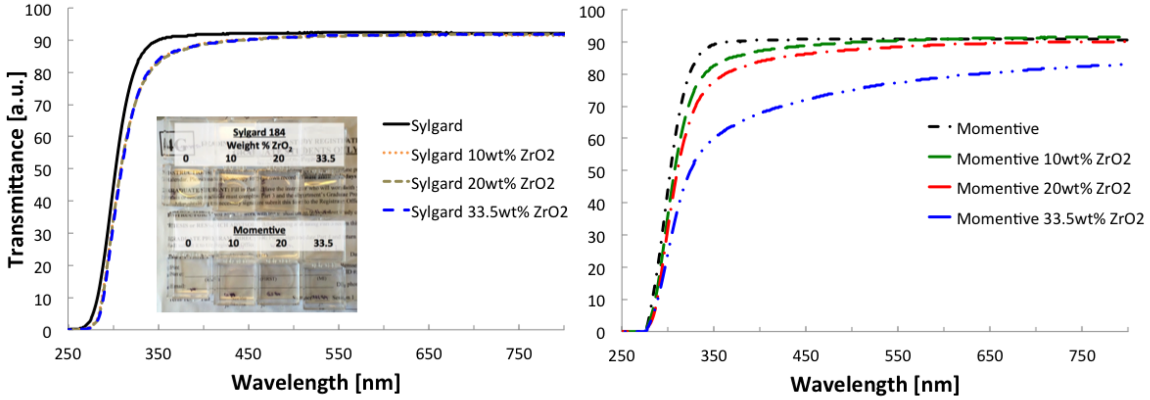

Figure 3.5. UV-vis transmittance data of silicone nanocomposite. (a) Sylgard system (methylated silicone). Inset showing transparency of both Sylgard and Momentive samples (b) Momentive system (methyl/phenyl silicone).

Since the peak wavelength of the RB LEDs is around 451 nm, the transparency was taken at 451 nm and compared as a function of silicone type and ZrO_2 loading in Table 3.2. While the transparency of the Sylgard-ZrO_2 system decreased slightly with increasing ZrO_2 concentration, the Momentive system showed a more significant decrease in transparency with increasing ZrO_2 loading, dropping from 89% to 72% transparency when increasing from 10 wt% to 33.5 wt% ZrO_2.

Table 3.2. Transparency of encapsulant as a function of silicone and ZrO_2 loading.

Silicone	ZrO_2 Loading [wt%]	Transparency [%]
Sylgard	0	92.1
Sylgard	10	90.4
Sylgard	20	90.2
Sylgard	33.5	90.1
Momentive	0	90.8
Momentive	10	88.9
Momentive	20	86.2
Momentive	33.5	72.1

3.3.3 Refractive Index - Ellipsometry

The Cauchy model fit to the raw ellipsometry data yielded the coefficients A, B [μm^2], C [μm^4], and the thickness of each sample. In Figure 3.6 the coefficients were taken and plotted against wavelengths from 400-700 nm for the Sylgard and Momentive nanocomposite systems using the well known Cauchy relation[30]:

$$RI(\lambda) = A + \frac{B}{\lambda^2} + \frac{C}{\lambda^4} \quad (3.2)$$

This was used to find the refractive index at 451 nm, which was subsequently tabulated and plotted as a function of ZrO_2 NP loading as seen in Table 3.3 and Figure 3.7 for both silicone systems.

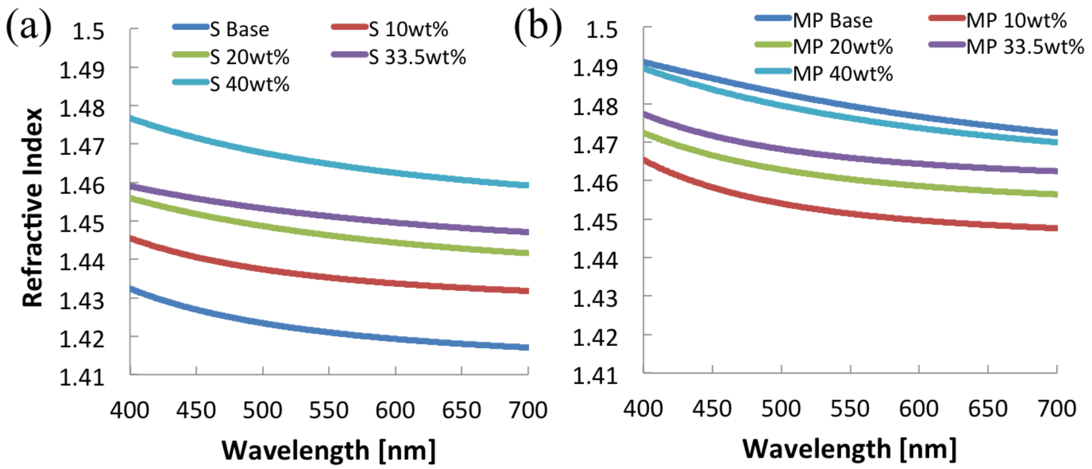

Figure 3.6. Cauchy model for the refractive index of (a) Sylgard-ZrO_2 and (b) Momentive-ZrO_2 nanocomposite materials and plain silicone.

While the Sylgard system shows an increase in RI with increasing ZrO_2 loading from 1.43 to 1.47 between the base Sylgard and 40 wt% (10.3 vol%) ZrO_2 loading, respectively, with a refractive index of 1.46 at 33.5 wt % (8 vol%), the Momentive system showed an initial decrease in RI from 1.49 for the base silicone to 1.48 for ZrO_2 loaded, with a RI of 1.47 at 33.5 wt% (8 vol%).

As a check on the testing method and analysis, the refractive index of the base Sylgard at 589 nm was found to be 1.42, which is 0.6% off the literature value of 1.4118 as claimed by the Dow Corning product information sheet for Sylgard 184.[22]

Table 3.3. Refractive index of silicone nanocomposite systems.

ZrO_2 Loading		Refractive Index		ΔRI [%]	
wt%	**vol%**	**Sylgard**	**Momentive**	**Sylgard**	**Momentive**
0	0	1.43	1.49	0	0
10	1.9	1.44	1.46	1.0	-1.9
20	4.1	1.45	1.47	1.7	-1.3
33.5	8.0	1.46	1.47	2.0	-1.0
40	10.3	1.47	1.48	3.1	-0.2

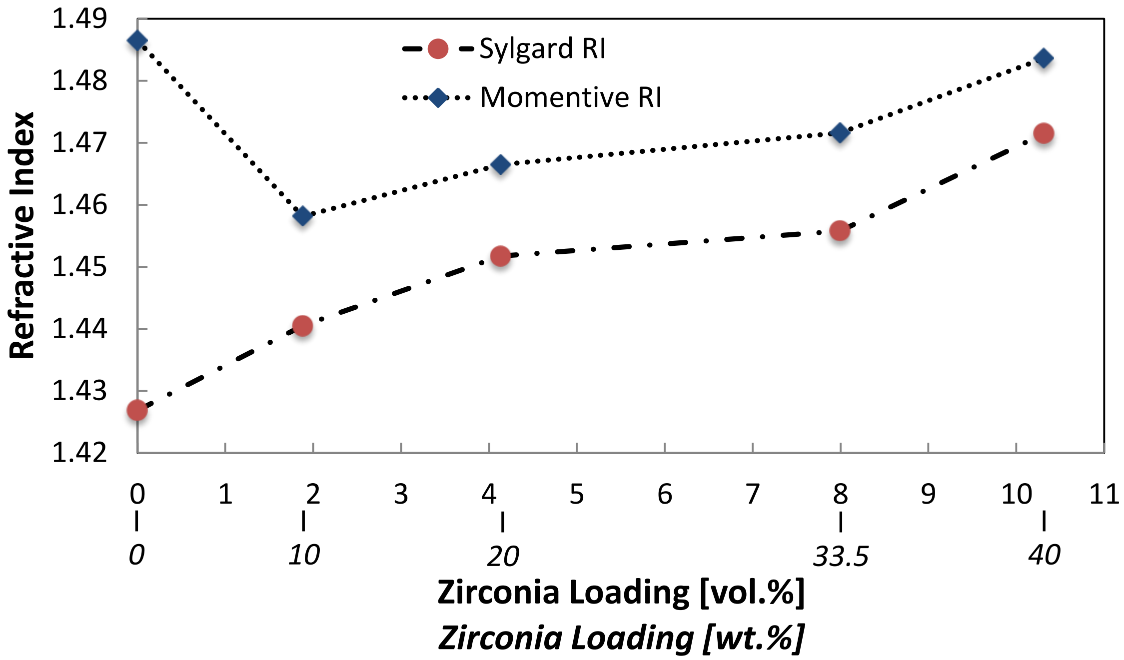

Figure 3.7. Refractive index as a function of ZrO_2 loading for Sylgard and Momentive Systems.

3.4 Spectral Output Power – Integrating Sphere

The raw spectral output power data in watts per nanometer [W/nm] as a function of wavelength can be used to analyze several different aspects of the LED samples and their respective conformal coating and encapsulant performance.

Samples are denoted with a B or RB to indicate Blue or Royal Blue. The number that follows indicates the LED number. An S or MP is used to indicate Sylgard or methyl phenyl Momentive silicone, respectively. The next indicator is a D or an O for Dow or Osram YAG. If a number follows the D or O it indicates the YAG loading. The last indicator is the zirconia loading in weight percent (typically 33.5 wt%). See Table 3.4 for conventions and examples that are used throughout this thesis and refer to the Appendix for a comprehensive description of the LED samples.

Table 3.4. Naming convention for LED samples and color convention for graphing.

Item	Naming Convention	Example	Description
LED Naming	LED_Silicone_YAG_ ZrO_2 wt%	RB29_MP_O_33.5	Royal Blue LED 29 with Momentive (methyl/phenyl) silicone, Osram YAG, 33.5 wt% ZrO_2 NPs
Graphing	Higher RI samples have blue markers, lower have red	In comparing silicones, MP is blue S is red, nanoparticle loadings: 33.5 wt% is blue and plain silicone is red, etc.	

3.4.1 Determination of Phosphor Required for White Light

To determine the appropriate YAG loading to achieve white light, different YAG loading fractions in silicone were tested. Initially, Blue LEDs were used with 5, 10, 15, and 65 wt% YAG:Ce from Dow. The output spectrum before and after addition of 10 wt% YAG is shown in Figure 3.8.

The spectrum and the picture included show a deficiency of phosphorescence spectrum. The loadings from 5-65 wt% were tested and mapped on the CIE 1931 colorspace to determine where along a line of loadings white light could be achieved, see Figure 3.9. From the colorspace the target YAG loading would be between 15 and 65 wt% for white light. However, while B10, B11, and RB12 were made in the same batch to test the value of 65 wt% YAG, RB12 provided good white light while B10 and B11 overshot the white point and produced yellow light, meaning that 65 wt% (27.55 vol%) YAG in plain silicone was ideal to produce white light when using the RB LEDs. It is important to note that both weight percent and volume percent are reported in this manuscript since the weight percent is used for calculations such as ZrO_2 loading when making a composite sample or for grafting density, while volume percent is needed since it is the volumetric amount of YAG that must remain constant from silicone-YAG to silicone-ZrO_2-YAG samples to yield the same white light output, because the weight percent value for YAG will decrease (due to inclusion of a third material and differing densities). From the spectra in Figure 3.10 it can be seen that while the Blue LEDs have a peak at 466 nm, the Royal Blue LEDs have a primary peak at about 451 nm, which corresponds to indigo, and a secondary peak at about 463 nm which corresponds to blue. Figure 3.10c shows a nice white, pcLED spectrum similar to that found in literature, Figure 3.10d. It should be noted that the primary indigo peak of ~450-451 nm is ideally suited to Ce doped YAG as it corresponds to the energy to excite an electron into the lowest d-level of the Ce^{3+} ions.[16]

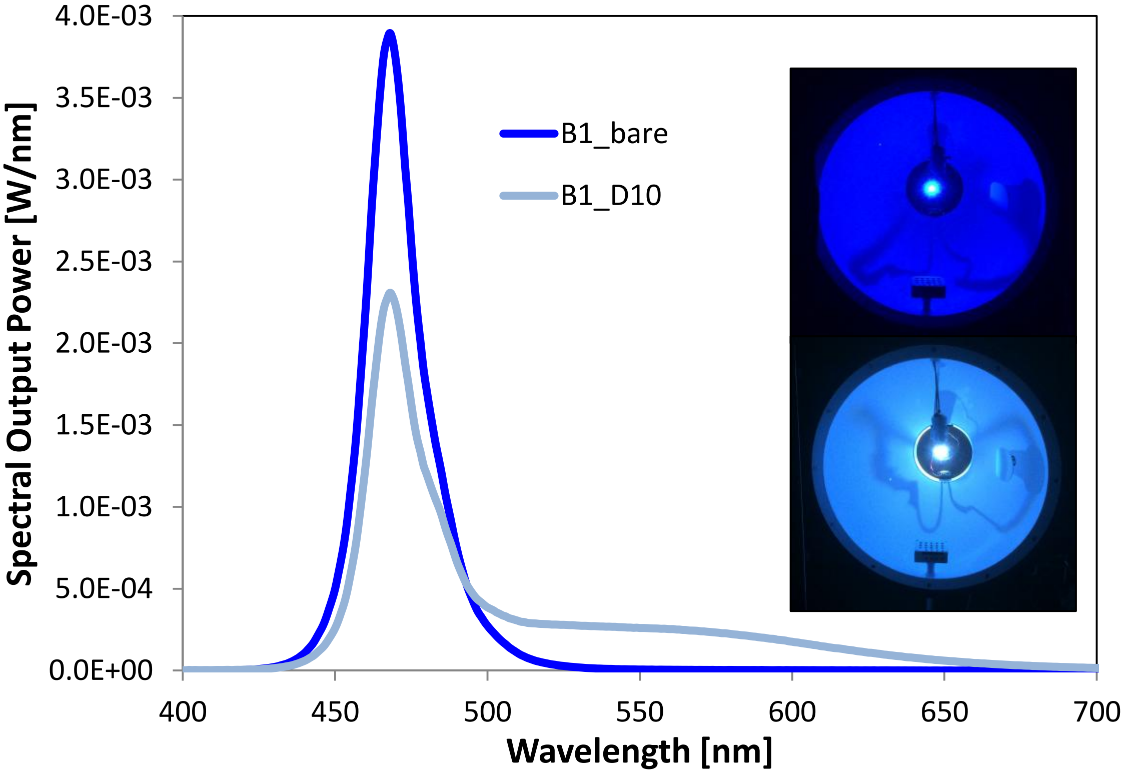

Figure 3.8. Blue LED using 10 wt% Dow YAG:Ce Phosphor. Picture of pre- and post- addition of YAG shown in inset.

After RB12 provided good, white light with 65 wt% Dow YAG, RB17 and RB18 were made. From Figure 3.9 it can be seen that repeatable results for color space coordinates, and thus LED color, were achievable with the solvent evaporation conformal coating placement. However, while the 65 wt% Dow YAG on RB LEDs provided good white light, when the Dow phosphor ran out and Osram was used with RB27, the new phosphor showed a much closer CIE 1931 coordinate to the ideal white point (0.33, 0.33) than was seen from prior samples.[27] This can be seen visually in Figure 3.11.

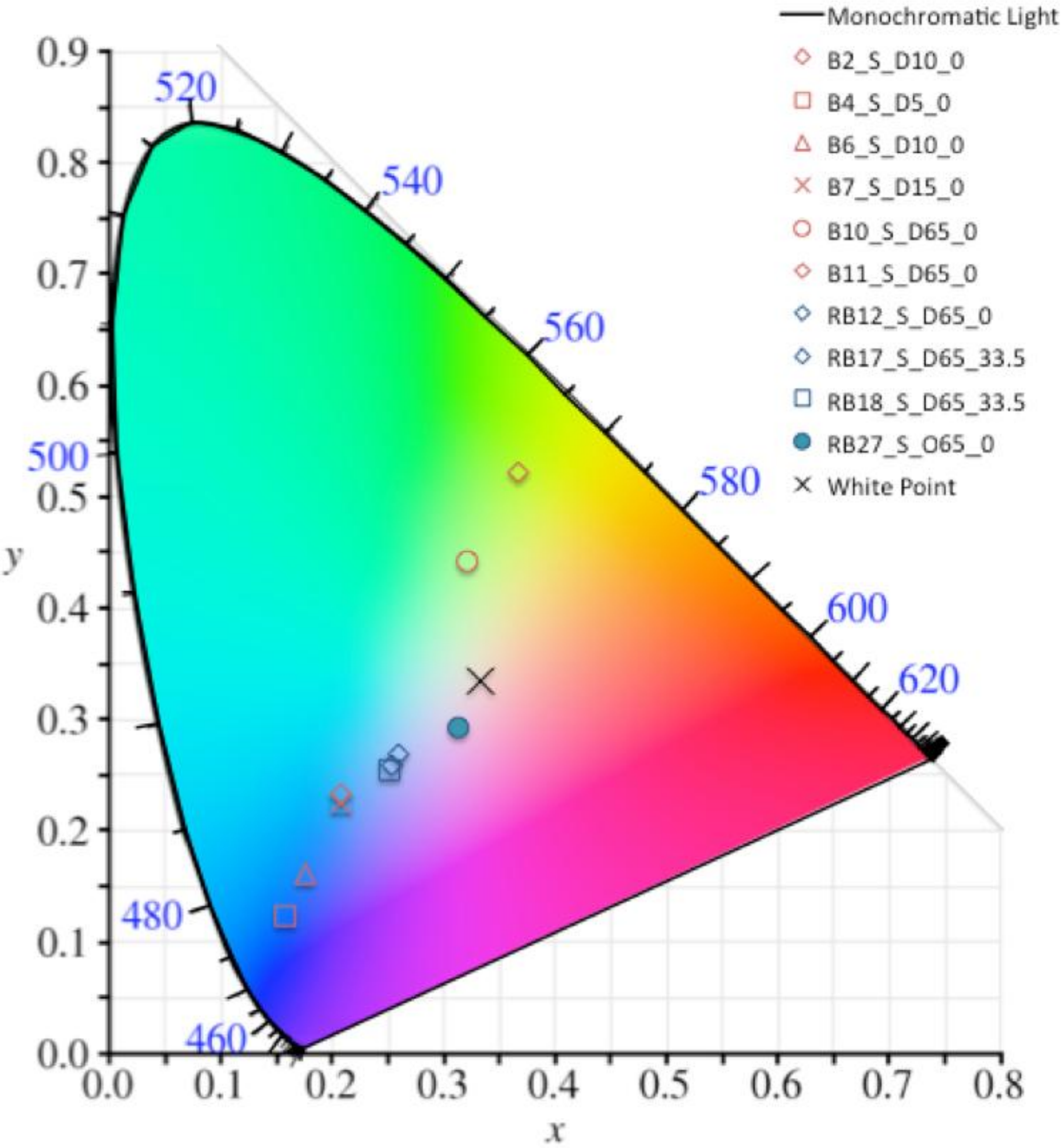

Figure 3.9. CIE 1931 for blue (B) and royal blue (RB) LED YAG loading determination. Red markers represent blue LEDs while blue markers represent royal blue.

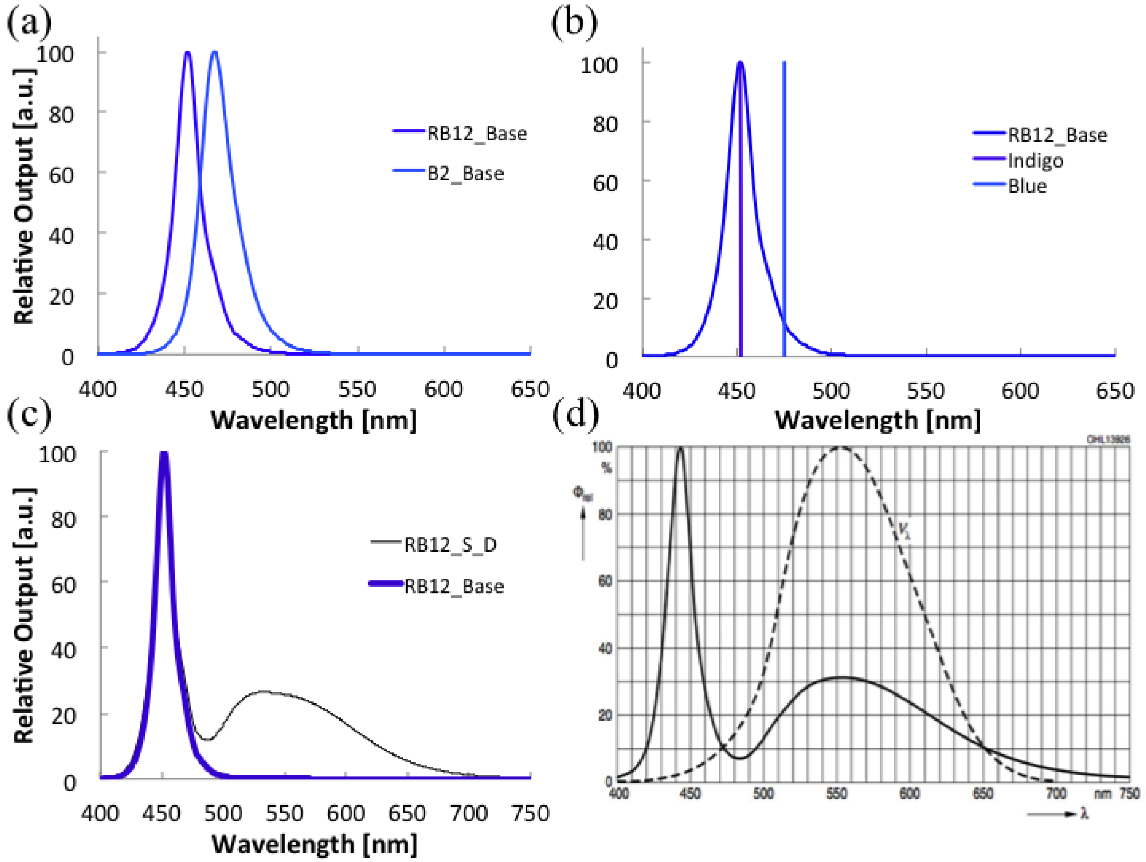

Figure 3.10. Blue vs. royal blue spectra and phosphor-converted white spectrum. (a) Unencapsulated LED spectra for blue and royal blue LEDs for comparison. (b) Wavelength locations for the 2 peaks that combine to make a royal blue LED. (c) RB12 before and after phosphor modification. Both curves were normalized by their respective maximum peak output for visualization. (d) Example white spectrum from YAG:Ce pcLED obtained from Ref. 39 and courtesy of OSRAM.[39]

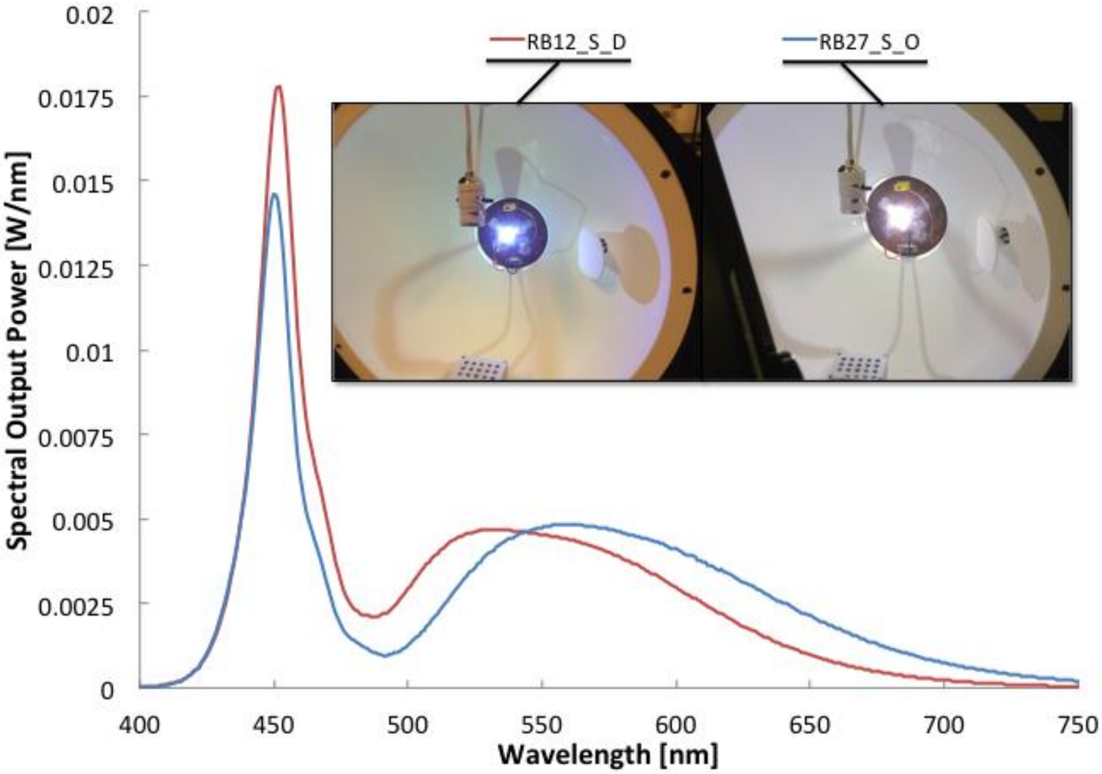

Figure 3.11. RB LEDs comparing Dow vs. Osram phosphors. Note how the juxtaposition of the images makes the blue in the Dow phosphor sample LED more apparent which can also be confirmed in Figure 3.9.

Thus it was seen from spectroscopic measurements that 65 wt% (27.55 vol%) YAG in silicone on Royal Blue LEDs provided the best white light. Moreover, the Osram YAG achieved close to the ideal white value, as seen in Figure 3.9 and Figure 3.11.

3.4.2 Light Extraction Efficiency

The light extraction efficiency of the nanocomposite encapsulated LEDs was investigated by taking an initial spectral output measurement for an LED and then another after adhering a dome of either the base silicone or ZrO_2 loaded nanocomposite, see Figure 3.12 for example spectra. From these spectra it can be seen that the phenylated Momentive silicone has a slightly higher increase in output compared to the methylated Sylgard silicone.

The ratio of the peak output post-modification to bare semiconductor was taken and plotted against the ZrO_2 loading fraction (Figure 3.12 (c)). From this it can be seen that the addition of the zirconia improves the light extraction efficiency for the Sylgard matrix initially, before dropping off between 20 wt% and 33.5 wt%. However, the inclusion of ZrO_2 into the MP matrix led to a stead decrease in LEE with increasing NP content. In previous work in our group, the blue LEDs did not show an improvement in light extraction efficiency, while there was a significant improvement in the red and green.[3] It should be noted that this was seen in systems with much higher zirconia loading than the 33.5 wt% used herein. In all cases, there was an increase in index of refraction. Thus, the reduction in efficiency in the MP system must be due to increased scattering and could be improved with further refinement of the composite processing. All samples, excluding the 33.5 wt% Sylgard sample, have a higher light extraction efficiency than a bare, unencapsulated LED, meaning that the silicone and silicone nanocomposite channel more light out than a bare semiconductor.

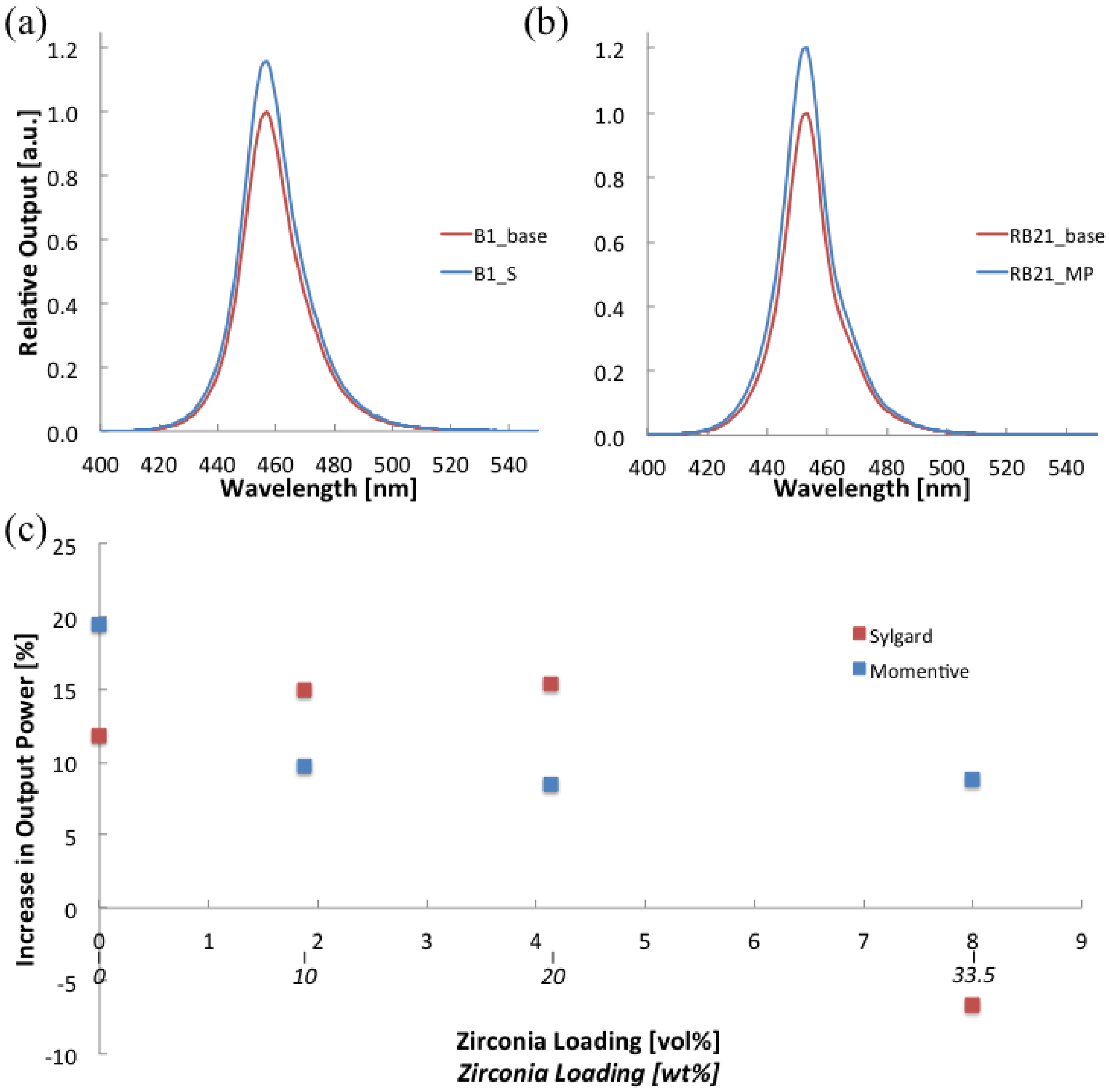

Figure 3.12. Light extraction efficiency. Normalized spectral output for (a) a plain Sylgard silicone encapsulated LED and (b) a plain Momentive encapsulated LED. (c) Increase in output power from bare LED output at 451 nm (LEE) as a function of ZrO_2 loading for both Sylgard and Momentive systems.

3.4.3 LED Aging

The relative output power of the Sylgard-based LED system, Aging Set 1, as a function of aging time can be seen in Figure 3.13. RB15 was used as an unaged control sample to compare against the aged samples. It should be noted that RB17 LED was damaged during testing after the 633 hours point and was unrecoverable. The aging parameters for the Aging Set 1 LEDs can be seen in Table 3.5. Over the aging period there was a small decrease in the output power for the original Aging Set 1. While the overall output for the LEDs in Aging Set 1 did not decrease significantly, a decrease in the phosphorescence spectrum can be seen with time, Figure 3.14.

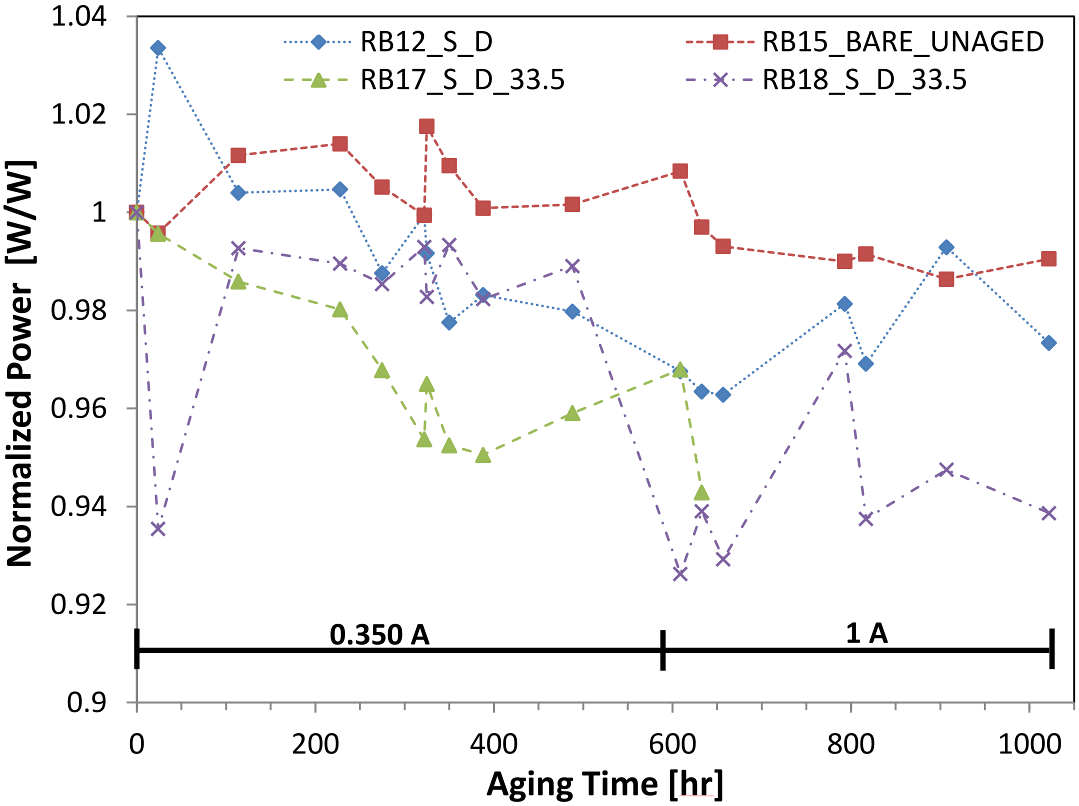

Figure 3.13. Aging set 1. RB12, RB17, and RB18 use Dow YAG. The lower black bars indicate the operating current for the Set 1 LEDs.

Table 3.5. Aging Set 1 aging parameters. The normalized output power was measured at the corresponding aging time prior to altering testing conditions.

LED	Aging Time [hrs]	Current [A]	Normalized Output Power
RB12	609	0.350	0.968
RB17	609	0.350	0.968
RB18	609	0.350	0.926
RB12	633	1.0	0.963
RB17	633	1.0	0.943
RB18	633	1.0	0.939
RB12	1140	1.5	0.998
RB18	1140	1.5	0.949

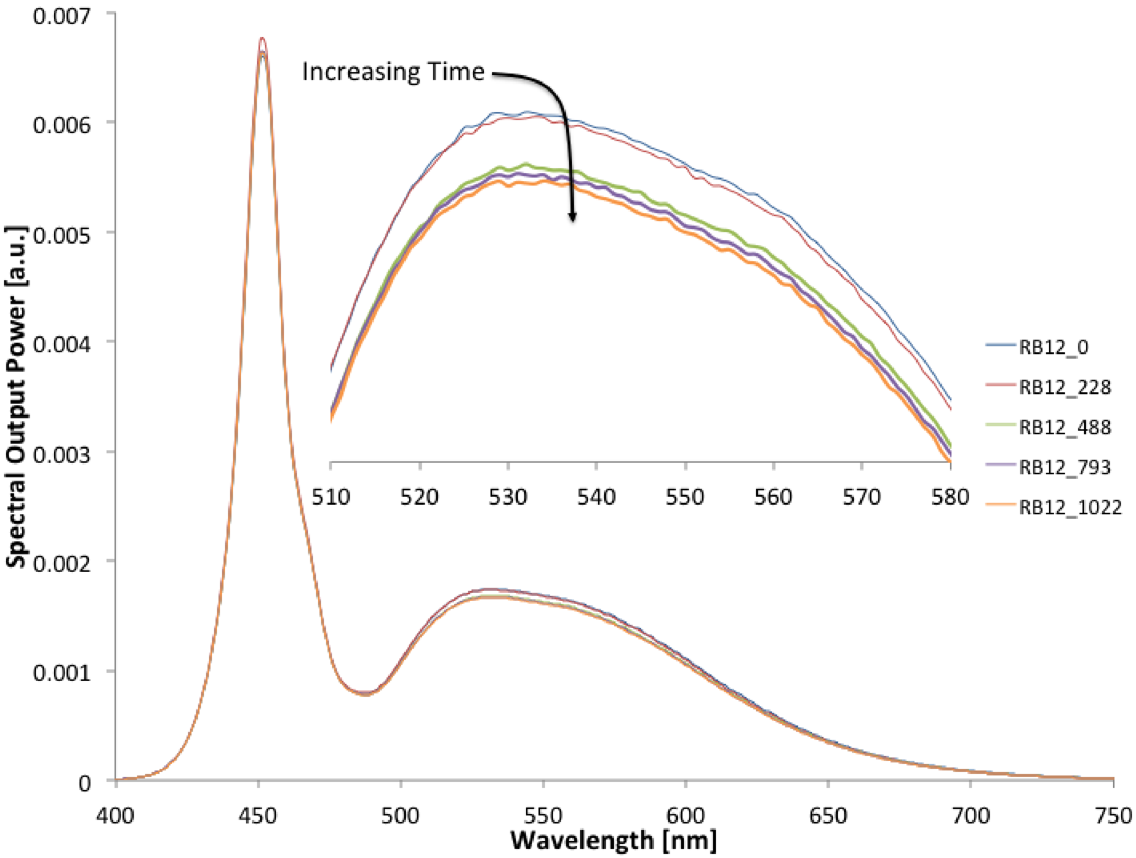

Figure 3.14. Spectral output decrease with aging for RB12. Inset shows decreasing phosphorescence spectrum with time.

The aging results for the higher refractive index MP LEDs as well as a new set of Sylgard samples is shown in Figure 3.15. Over the 500 hours aging at 1.5 A the MP samples showed little degradation in output power, with RB30 and RB40 retaining 99% of their initial output, while the Sylgard samples showed a loss in output power of 94% and 88% for RB35 and RB36, respectively.

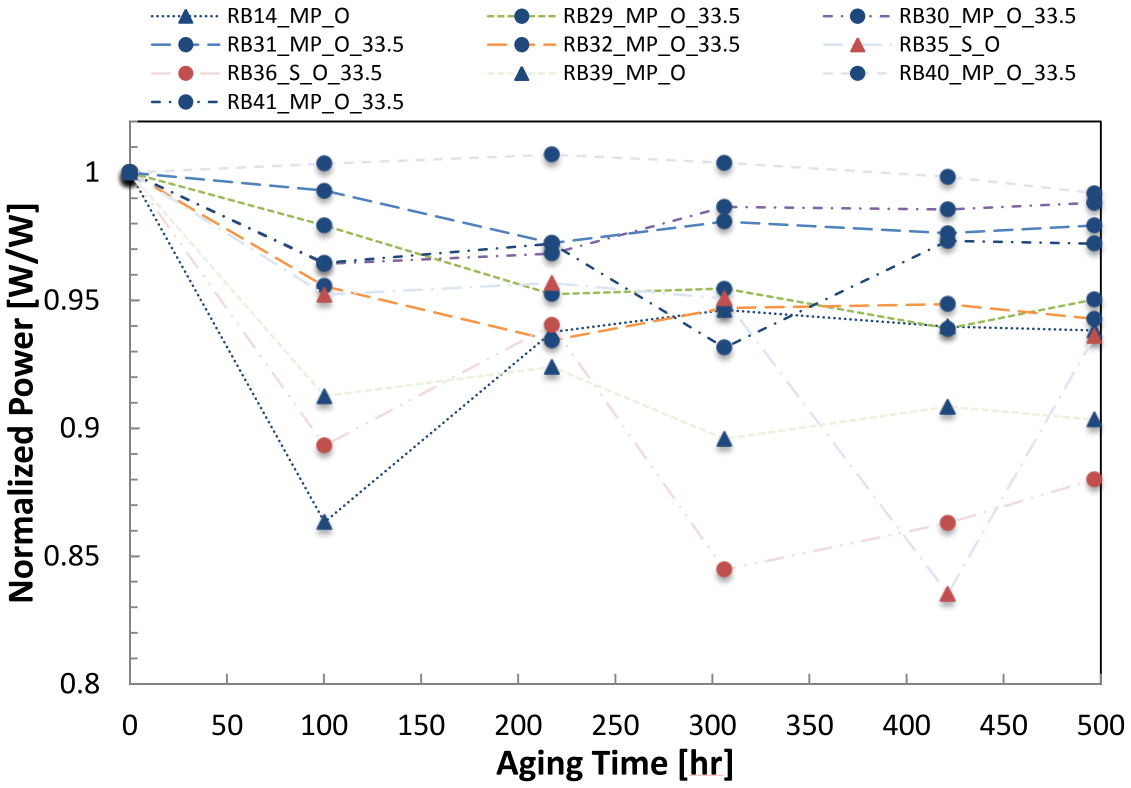

Figure 3.15. Preliminary aging test on LED Set 2: all samples. Marker shape denotes nanoparticle loading: circle for NPs, triangle for base silicone, marker fill denotes silicone used, red = Sylgard, blue = MP.

3.4.3.1 PCE as a Function of LED Aging

The phosphor conversion efficiency as a function of aging time was tracked along with the output power. Figure 3.16 shows the progress for the Sylgard-ZrO_2 LEDs which used Dow YAG while Figure 3.17 shows Aging Set 2 LEDs which include the Momentive silicone system as well as a set of Sylgard samples for comparison under the further enhanced power conditions, both of which used the Osram YAG. The phosphor used is important to note since its spectral response and any quenching phenomena can be associated with different Ce^{3+} content, impurity concentration, and size.[40–43] Overall, the

Aging Set 1 Sylgard samples with 33.5 wt% ZrO_2 had and maintained a higher PCE, around 10% or greater enhancement, than the samples with the plain, base silicone (RB12).

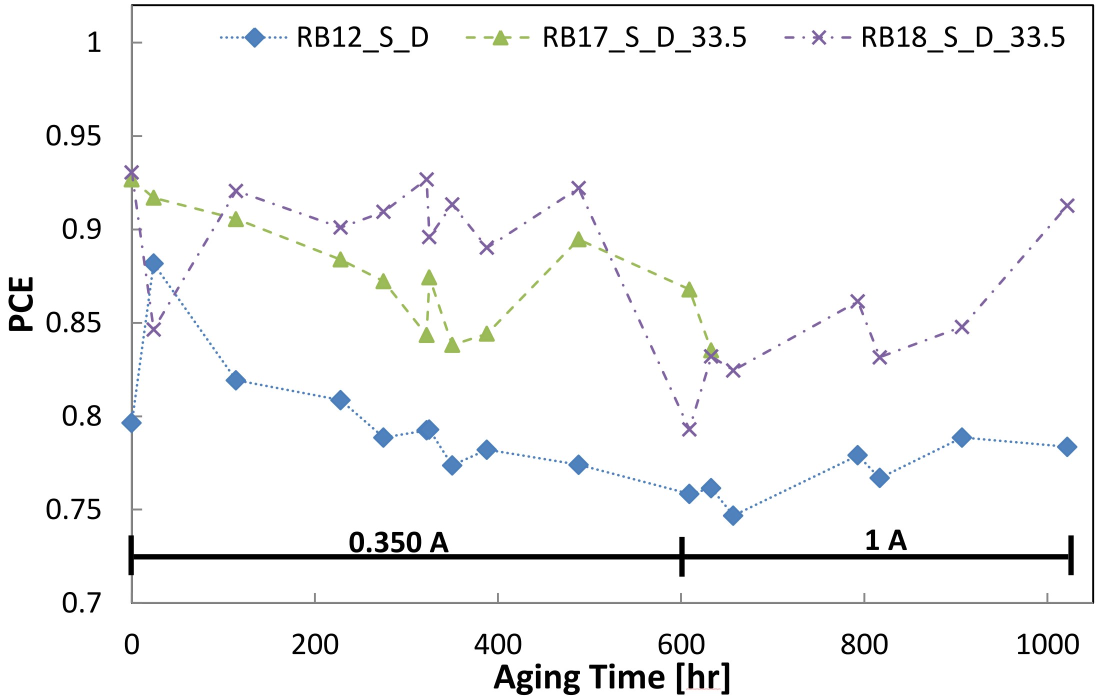

Figure 3.16. Phosphor conversion efficiency for Aging Set 1 - Sylgard system. The black bar corresponds to aging current for RB12, RB17, and RB18.

But for the exception of the anomalous dip in RB18's PCE value at 609 hours, the PCE for the two LEDs with the nanocomposite stayed several percentage values higher than the LED without.

In assessing the PCE of the higher RI higher thermal conductivity Momentive (MP) silicone, it can be seen that the PCE for the MP silicone was enhanced by 10% or greater over that of the Sylgard (S) samples over the 500 hr aging period of the Aging Set 2 LEDs. However, within the same-type silicone samples there was negligible difference between the PCE of the plain, base silicone and that of the nanocomposite

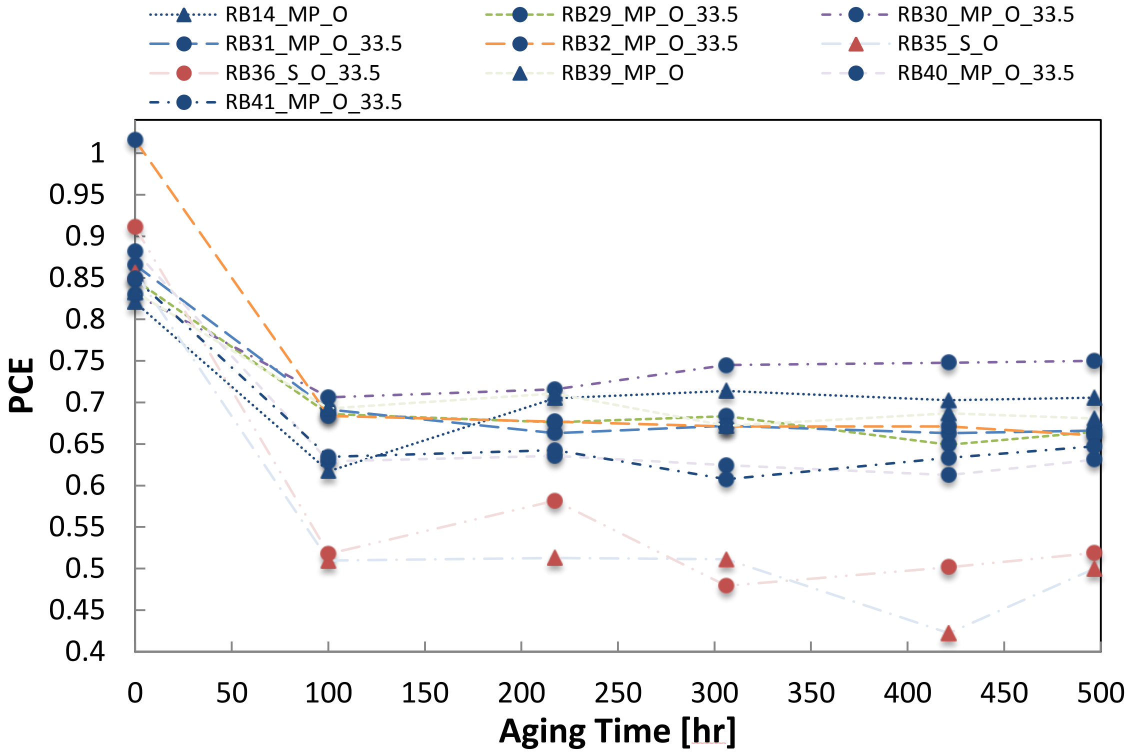

Figure 3.17. Phosphor conversion efficiency of Aging Set 2. Both Sylgard and Momentive samples aged at 1.5A for 500 hours. Marker shape denotes nanoparticle loading: circle for NPs, triangle for base silicone, marker fill denotes silicone used, red = Sylgard, blue = MP.

4. Discussion

4.1 Nanoparticle Synthesis and Functionalization

The ~5 nm size of the nanoparticles obtained was small enough to avoid significant transmittance losses due to Rayleigh scattering and was of a comparable size to that obtained in prior studies.[3,26,44] The TGA and FTIR results, and subsequent successful dispersion of NPs in silicone, confirmed a bimodal grafting distribution was achieved. However, even though successful grafting was achieved, the MP system suffered from a lower graft density compared to the methyl system. While the methyl system had an effective graft density of 0.36 brushes/nm^2, with 68% coming from the 1k PDMS and 32% from the 10k PDMS, the MP system has an effective graft density of 0.21 brushes/nm^2, with 89% from 1k PDMs while only 11% of the graft density came from 10k MP brushes. Although good transparency in the optical spectrum for the methylated silicone system, with only minor decreases due to inclusion of ZrO_2, was observed, a significant decreasing transparency with increasing NP concentration occurred with the MP silicone system.

One potential source of this decrease in transparency may be due to compatibility between the MP brushes on the nanoparticle and the MP matrix used. A key criterion for two copolymers to be compatible for complete, homogeneous mixing is that they share relatively similar interaction parameters.[45,46] The easiest way to achieve this is to have two copolymers with the same side groups in similar proportions. Since the MP silicone used as brushes was not available as a matrix material, Momentive provided us with two different potential matrix materials that should be compatible with the brushes. However, when the original, unmodified brushes were mixed in with the matrix and the crosslinking agent and catalyst were added the resulting sample was opaque. While this may be an indication of incompatibility, it is also possible that the platinum catalyst and crosslinking agent initiated a dehydrogenative coupling crosslinking, whereby the hydroxyl groups at the end of the brushes participate in crosslinking with the hydride functional HMS-301, producing hydrogen gas, which would lead to microbubbles that resulted in a lack of transparency.[47] The release of hydrogen gas is why dehydrogenative coupling is used to produce foamed silicone-based materials, where transparency is not a priority, yet presents issues when making LED encapsulants.[47] With this being a potential source of loss in transparency, it is possible that some of the grafted 10k MP brushes had hydroxyl groups left over after the phosphate modification step leading to a similar result when NPs with these 10k brushes were mixed with the matrix, crosslinking agent, and Pt catalyst.

However, since the silicones from Momentive were from their proprietary selection and detailed properties of the matrix material and brushes were not available, the compatibility claim was left to question. Without this knowledge it is possible that the brushes and matrix are not completely miscible, and, while the grafted nanoparticles and matrix are transparent independent of one another, the two experience some amount of phase separation leading to a loss in transparency when mixed.

Another possible cause of the loss in transparency with increasing NP loading is related to the nature of the surface coverage and makeup of the polymer brushes on the nanoparticle. The original bimodally grafted ZrO_2 NPs were covered in brushes with a similar chemical makeup to the matrix material, with both 1k- and 10k-PDMS having only methyl side groups along the polymer backbone, and a graft density of 0.11 brushes/nm^2 for the 10k brushes. Contrastingly, the bimodal NP system using the 10k MP brushes were covered in 1k PDMS brushes that were very different from the matrix material due to the lack of phenyl side groups along the backbone, and only had a graft density of 0.02 brushes/nm^2 for the 10k MP brushes.

The similarity between the two types of brush and the matrix for the methylated silicone system leads to insensitivity to variance of one type of brush or the other when considering polymer miscibility, as both are compatible with the matrix. On the other hand, assuming the 10k MP brushes are compatible with the Momentive matrix material, the 1k PDMS brushes are most likely not due to the lack of phenyl side groups along the backbone. It is possible that the lower graft density of 10k MP brushes leaves the 1k brushes exposed to interact with the matrix, leading to some amount of phase separation. While further investigation into the effect of low 10k MP graft density on the interaction between short 1k brushes and the Momentive matrix material were beyond the scope of this study, the graft density of the longer brushes for both systems may provide further insight into potential problems.

It was shown previously that in order to achieve good dispersion of the 1k, 10k PDMS grafted ZrO_2 nanoparticles in the Sylgard matrix, the graft density of the longer 10k brush needed to be greater than 0.04 brushes/nm^2.[3] While this criteria is clearly met for the methylated silicone system, the MP system has less than half of the long brush density required for good dispersion, assuming the Momentive matrix material has the same molecular weight as the Sylgard matrix. However, since the molecular weight of the Momentive matrix was not known, if it is not similar to the Sylgard system it is difficult to speculate further based on this longer brush graft density criteria.

While the smaller graft density of 10k MP brushes would be desirable, as it would mean larger loading of ZrO_2 cores per unit volume could be achieved in a given composite sample, it would also mean there are fewer MP brushes to aid in entanglement with the matrix material as well as potentially allowing more of the incompatible 1k brushes to interact with the MP matrix, yielding phase separation or other dispersion issues.

Since further investigation was beyond the scope of this work, the demonstrated higher RI with the MP silicone warrants further investigation into using the MP system.

4.2 Thermal Conductivity Measurements

The addition of the bimodally grafted ZrO_2 NPs caused an increase in the thermal conductivity of the Sylgard silicone. This came as no surprise as it can be seen in Figure 3.4 that the nanocomposite approximately followed the well known additive rule of mixtures (RoM) relationship[48]:

$$k_{comp} = v_{ZrO_2} k_{ZrO_2} + v_{silicone} k_{silicone} \tag{4.1}$$

where the composite thermal conductivity, k_{comp}, is a weighted average of the thermal conductivities of each component: the ZrO_2 NPs, k_{ZrO_2}, and the silicone, $k_{silicone}$, which are scaled by their volume fraction contributions v_{ZrO_2} and $v_{silicone}$, respectively. While the measured k_{comp} was observed to exceed the RoM relationship by inclusion of 33.5 wt% (8 vol%) ZrO_2 NPs, the RoM relationship was within the error of the measurements.

The thermal conductivity of polymers at room temperature is typically between 0.14 W/mK for polystyrene and 0.44 W/mK for high density polyethylene.[48] This is relatively low compared to the thermal conductivity of typical filler particles such as zirconia or diamond nanoparticles, or carbon nanotubes (CNTs) with thermal conductivities of 2.7, 2000, and 6000 W/mK, respectively.[48] Unfortunately, CNTs would yield and opaque composite and diamond nanoparticles would be prohibitively expensive and difficult to disperse homogeneously. On the other hand, ZrO_2 NPs are optically transparent, comparatively less expensive, and readily dispersible in encapsulant materials via the bimodal brush technology described here.

While the up to tenfold enhancement in the thermal conductivity of polymer micro- and nanocomposites that has already been shown for other polymer-nanoparticle systems would be highly desirable for keeping the LEDs and phosphors from heating up, these systems are typically opaque since optical clarity is not necessary for the targeted technology and achieving good dispersion of particles has been an issue.[29,49] Meanwhile, nanocomposites with enhanced thermal conductivity that maintain transparency, such as the cellulose nanofiber-epoxy system mentioned previously, have been discovered and studied. Yet the 28% increase in thermal conductivity and maximum transparency of 80% at a 58 wt% cellulose nanofiber loading, means a 20% transmittance loss tradeoff for increasing thermal conductivity, leaving much room for improvement. On the other hand, the 81% increase in thermal conductivity with only 8-10% transparency lost at 33.5 wt% (8 vol%) ZrO_2 in silicone presents the possibility of higher thermal conductivity, optically transparent composites that may in time get closer to the tenfold enhancement in thermal conductivity seen in their opaque counterparts.

The increase in thermal conductivity of the encapsulant presents promise, in that it means that the composite can mitigate the issue of heating at the semiconductor die and in the phosphors, leading to a cooler semiconductor and phosphor and thus an increase in efficiency of both.

4.3 Refractive Index - Ellipsometry

While the increase in RI of the methylated Sylgard system with increasing NP loading was demonstrated in prior works, the drop in RI with inclusion of NPs then subsequent increase with increasing loading fraction of ZrO_2 in the MP-Momentive system was perplexing.[3]

The one property provided along with the MP brushes and matrix material was the methyl-to-phenyl ratio of each. It was known that the matrix material had a lower methyl-to-phenyl ratio than the grafted brushes, meaning that the matrix would have a higher refractive index than the brushes, since the refractive index will increase with increasing phenyl substitutions.[50] Yet while the methylated silicone showed a 1% increase in RI from 0 wt% to 10 wt% (0 vol% to 1.9 vol%) the MP system showed a 2% decrease over the same range. While it would be tempting to attribute this to the same issues plaguing the transparency of the MP silicone system, there was an increase in RI with increasing NP loading, inverse of the decrease in transparency.

While the brushes on the ZrO_2 in the MP system replace some of the higher RI matrix with lower RI brushes (both the 1k and 10k MP), yielding a decrease in RI, the inclusion of ZrO_2 cores would yield an increase in RI. Thus the change in refractive index would be a complex combination of the decrease from replaced matrix material and increase with ZrO_2 loading.

4.4 Light Extraction Efficiency

The decreased LEE with ZrO_2 loading was expected as it had already been discovered in prior work.[3] This can be explained through the absorption of blue light in the ZrO_2 nanocomposite by small molecules, which can be seen in UV-Vis transmittance trends in Figure 3.5. However, increases in LEE at red and green wavelengths due to the inclusion of ZrO_2 NPs would mean that, while less light is extracted from the blue part of the pcLED spectrum, increasing amounts of light are extracted as the wavelength increases into the phosphorescence portion of the spectrum.

Previously, it had been shown that inclusion of ZrO_2 NPs provided a smaller increase in LEE compared to using plain silicone as an encapsulant for blue LEDs.[3] However, the ZrO_2 content of the Blue LED encapsulant was much higher since a matrix-free system was being used and the LED used was blue, with a wavelength around 460 nm, instead of royal blue, with at wavelength around 450 nm. From the transmittance data it can be seen that more light will be lost as the wavelength is decreased and the ZrO_2 content is increased. Since silicones for optical applications are required to have 99% or greater transparency in the visible spectrum at a sample thickness of 1 mm, the cause of this loss in transparency for the Sylgard system can be ascribed to the ZrO_2.[14] However, we expect an increase in LEE with increasing refractive index since there would be a reduction in the Fresnel reflection losses at the interfaces.[1,14] While the Sylgard system initially exhibited such an increase, at the highest loading achieved in this study there was actually a loss in LEE and, counter to expectation, the Momentive silicone showed a decrease with increasing ZrO_2 content, potentially due to absorption from small molecules.

4.5 LED Aging

While there was no significant enhancement in aging properties for the Sylgard silicone LEDs in Aging Set 1 over the 1000 hour aging study, there were no deleterious effects of including the nanoparticles. Aging Set 2 clearly illustrates that the Momentive-based LED samples experienced less of a decrease in power output over the 500 hour period at 1.5 A compared to the Sylgard based samples. Since the spectral output of the LEDs was measured using the recommended 0.35 A, the testing pump current can be ruled out for explaining this increase in normalized power output over time, leaving the encapsulant material as the source for this enhancement. As seen with the first aging samples, there was no significant difference in the aging properties of the Sylgard-based LEDs between the base, plain silicone and the ZrO_2 loaded silicone in the second set. On the other hand, among the six ZrO_2 loaded Momentive samples and the 2 base, plain Momentive LEDs, the ZrO_2 loaded ones maintained an overall higher power output than the base samples, with four preserving near to 100% and two reducing only to 95% of their output while the base silicone samples dropped as far as 90%, with a max of 95% output, over the 500 hours. It is well known that some methyl groups can be replaced by phenyl groups to improve the thermal stability and refractive index of silicones while still maintaining the desired properties of flexibility and durability that PDMSs offer.[47,50,51]

Thus, the enhancement in aging properties of the methyl-phenyl samples over the methylated Sylgard ones can most likely be attributed to a combination of the increased thermal conductivity and refractive index due to both the addition of phenyl side groups as well as high refractive index and thermally conductive ZrO_2 nanoparticles.

4.6 Phosphor Conversion Efficiency

The PCE for the Sylgard nanocomposite was higher than the base Sylgard over the 1000 hours aging period for Aging Set 1. Meanwhile the Momentive silicone LEDs in Aging Set 2 had a higher PCE than the Sylgard samples run in parallel over the 500 hours at 1.5 amps. Unlike Aging Set 1, there was no significant enhancement in PCE seen between the base plain silicone and ZrO_2-filled silicone samples among the same silicone system in this second set of LEDs. The purpose of including Sylgard samples in the Aging Set 2 LEDs was to have comparable units at the further enhanced current rating, since the Aging Set 1 LEDs were run at lower currents and with the Dow phosphor. While at 0.35 A the zirconia loaded Sylgard samples held a higher PCE over the base silicone, at 1.5 A no significant difference in PCE was seen for among the Sylgard samples. This may provide insight into why the Momentive samples did not exhibit a noticeable difference in PCE with inclusion of the nanoparticles. Thus, it would be insightful to conduct an aging and PCE study on Momentive based samples at the typical maximum power condition of 0.35 A to see if the operating current caused this discrepancy.

Originally it was thought that any enhancement seen in PCE would be a combination of the increased thermal conductivity, increased LEE, and increased RI, however, as seen in Figure 3.12, the LEE for the nanocomposite at 33.5 wt% is actually lower than for the base silicone. This is attributed to the loss of transparency due to absorption at the blue end of the spectrum.[3] It is possible that the increase in LEE seen in the Sylgard samples at lower loadings is due to the increase in RI while only minor absorption by small molecules is occurring. If this is the case, then a crossover occurs between 20 wt% and 33.5 wt% (4.1 vol% and 8 vol%) zirconia content at which the reduction in output due to absorption exceeds the gain from increased RI and an overall drop in LEE occurs.

The increasing transparency with increasing wavelength, and subsequent increasing LEE, would mean less blue yet more phosphorescence photons escaping the encapsulant due to the inclusion of ZrO_2 NPs. Since the PCE is determined by taking the ratio of the phosphorescence power to the difference in initial and final blue output, refer to Equation 2.3, the decrease in final blue output and increase in phosphorescence would lead to a larger value in the numerator and denominator of this ratio. Whether or not this difference balances out would have to be determined by either correlating the LEE or transmittance as a function of wavelength and the output spectra to fully assess the interplay of these phenomena on the spectral output power of the blue and phosphorescence portions of the spectral data and therefore potentially account for this complex behavior.

It is interesting to note that, for the Sylgard-based Aging Set 1 LEDs the inclusion of zirconia lead to an increase in PCE with no significant increase in relative output power, while the Momentive-based LEDs of Aging Set 2 showed potentially enhanced aging properties with inclusion of ZrO_2 yet no significant difference in PCE between the plain silicone and nanoparticle loaded encapsulants.

5. Future Work

The higher refractive index MP silicone system from Momentive shows potential with its higher refractive index, enhanced phosphor conversion efficiency and output, and better aging characteristics such that it warrants further pursuit in studying the system. If the cause of the excessive loss in transparency of the MP-ZrO_2 system compared to that seen from the Sylgard-ZrO_2 system can be determined and remedied, then there is great potential to increase the aging characteristics, spectral output (LEE), and PCE of pcLEDs.

6. Conclusions

Zirconia nanoparticles were successfully synthesized and modified such that a refractive index and thermal conductivity enhancement could be achieved with their inclusion in the commercially available Sylgard silicone. While a decrease in light extraction efficiency and transmittance was seen at the highest ZrO_2 content the overall aging behavior was promising. The increase in thermal conductivity with increasing composite composition was significant. This along with the increasing refractive index means that more light can be channeled out of the light emitting diode, phosphor, and encapsulant due to a larger escape cone as well as more heat being channeled away from the phosphors and semiconductor chip, allowing them to cool down, mitigating the issues of light lost to reduced phosphor quantum conversion efficiency, scattering, and internal reflection.

While no significant enhancement in the spectral output power of these methylated Sylgard silicone samples was seen due to the addition of ZrO_2 nanoparticles, their inclusion was shown not only to not be detrimental to the output power over time but in fact to yield a 10% or greater enhancement in phosphor quantum conversion efficiency in the Sylgard samples.

In using a higher-RI phenylated silicone from Momentive, better aging and phosphor conversion efficiency properties were achieved independent of ZrO_2 content, yet within the Momentive methyl-phenyl samples it appeared that the ZrO_2 loaded encapsulants may have performed better over the 500 hours at a higher current than their base silicone counterparts.

The promising properties of high refractive index, high thermal conductivity polymer nanocomposites for LED encapsulation observed in this investigation present proof for the applicability of these composites toward the enhancement in efficiency and subsequent reduction in energy waste for light emitting diodes, allowing for smaller, readily manufacturable, and more efficient solid state lighting units to be realized.

7. References

(1) Mont, F. W.; Kim, J. K.; Schubert, M. F.; Schubert, E. F.; Siegel, R. W. High-Refractive-Index TiO_2-Nanoparticle-Loaded Encapsulants for Light-Emitting Diodes. *J. Appl. Phys.* **2008**, *103*, 1-6.

(2) Tao, P. Epoxy and Silicone Optical Nanocomposites Filled with Grafted Nanoparticles. Ph.D. Dissertation, Rensselaer Polytechnic Institute, Troy, NY, 2012.

(3) Li, Y. Highly Integrated Surface Ligand Platform for Multifunctional Polymer Nanocomposites and Their Applications in LED Lighting. Ph.D. Dissertation, Rensselaer Polytechnic Institute, Troy, NY, 2014.

(4) Bardsley, N.; Bland, S.; Pattison, L.; Pattison, M.; Stober, K.; Welsh, F.; Yamada, M. *Solid-State Lighting Research and Development Multi-Year Program Plan*; Solid-State Lighting Program, U.S. Department of Energy, Office of Energy Efficiency and Renewable Energy: Washington, DC, 2014.

(5) Schubert, E. F. *Light-Emitting Diodes*, 2nd ed.; Cambridge University Press: New York, NY, 2006.

(6) So, F.; Kido, J.; Burrows, P. Organic Light- Emitting Devices for Solid-State Lighting. *Mrs Bull.* **2008**, *33*, 663–669.

(7) Lunia, A. K.; Patra, S. K.; Kumar, S.; Singh, S.; Pal, S.; Dhanavantri, C. Theoretical Analysis of Blue to White down Conversion for Light-Emitting Diode Light with Yttrium Aluminum Garnet Phosphor. *J. Photonics Energy* **2014**, *4*, 1-11.

(8) Zhang, L.; Li, B.; Lei, B.; Hong, Z.; Li, W. A Triphenylamine Derivative as an Efficient Organic Light Color-Conversion Material for White LEDs. *J. Lumin.* **2008**, *128*, 67–73.

(9) Krames, M. R.; Shchekin, O. B.; Mueller-Mach, R.; Mueller, G. O.; Zhou, L.; Harbers, G.; Craford, M. G. Status and Future of High-Power Light-Emitting Diodes for Solid-State Lighting. *IEEE/OSA J. Disp. Technol.* **2007**, *3*, 160–175.

(10) Allen, S. C.; Steckl, A. J. A Nearly Ideal Phosphor-Converted White Light-Emitting Diode. *Appl. Phys. Lett.* **2008**, *92*, 120–123.

(11) Narendran, N.; Gu, Y.; Freyssinier-Nova, J. P.; Zhu, Y. Extracting Phosphor-Scattered Photons to Improve White LED Efficiency. *Phys. Status Solidi Appl. Mater. Sci.* **2005**, *202*, 60–62.

(12) Kim, J. K.; Luo, H.; Schubert, E. F.; Cho, J.; Sone, C.; Park, Y. Strongly Enhanced Phosphor Efficiency in GaInN White Light-Emitting Diodes Using Remote Phosphor Configuration and Diffuse Reflector Cup. *Japanese J. Appl. Physics, Part 2 Lett.* **2005**, *44*, 649–651.

(13) Kim, J. K.; Chhajed, S.; Schubert, M. F.; Schubert, E. F.; Fischer, A. J.; Crawford, M. H.; Cho, J.; Kim, H.; Sone, C. Light-Extraction Enhancement of GaInN Light-Emitting Diodes by Graded-Refractive-Index Indium Tin Oxide Anti-Reflection Contact. *Adv. Mater.* **2008**, *20*, 801–804.

(14) Ma, M.; Mont, F. W.; Yan, X.; Cho, J.; Schubert, E. F.; Kim, G. B.; Sone, C. Effects of the Refractive Index of the Encapsulant on the Light-Extraction Efficiency of Light-Emitting Diodes. *Opt. Express* **2011**, *19*, A1135-A1140.

(15) Keppens, A.; Zong, Y.; Ohno, Y.; Dceoninck, G.; Hanselaer, P. Determining Phosphors' Effective Quantum Efficiency for Remote Phosphor Type LED Modules. In *Proceedings of CIE Expert Symposium on Spectral and Imaging Methods for Photometry and Radiometry*, Bern, Switzerland, Aug 30-31, 2010; National Institute of Standards and Technology: Gaithersburg, MD, Dec 1, 2010, 39-42.

(16) Bachmann, V. M. Studies on Luminescence and Quenching Mechanisms in Phosphors for Light Emitting Diodes. Ph.D. Dissertation, Universiteit Utrecht, Leipzig, Germany, 2007.

(17) Pankove, J. I. *Optical Processes in Semiconductors*; Dover Publications, Inc.: Mineola, NY, 1971.

(18) Light Emitting Diodes. *Kirk-Othmer Encyclopedia of Chemical Technology* [Online]; John Wiley & Sons, Posted July 15, 2005. http://dx.doi.org/10.1002/0471238961.1209070811091908.a01.pub2 (accessed Aug 10, 2014).

(19) Tao, P.; Li, Y.; Rungta, A.; Viswanath, A.; Gao, J.; Benicewicz, B. C.; Siegel, R. W.; Schadler, L. S. TiO_2 Nanocomposites with High Refractive Index and Transparency. *J. Mater. Chem.* **2011**, *21*, 18623.

(20) Caseri, W. Inorganic Nanoparticles As Optically Effective Additives for Polymers. *Chem. Eng. Commun.* **2008**, *196*, 549–572.

(21) Shimazaki, Y.; Miyazaki, Y.; Takezawa, Y.; Nogi, M.; Abe, K.; Ifuku, S.; Yano, H. Excellent Thermal Conductivity of Transparent Cellulose Nanofiber/epoxy Resin Nanocomposites. *Biomacromolecules* **2007**, *8*, 2976–2978.

(22) *Sylgard® 184 Silicone Elastomer*; Datasheet Form No. 11-3184B-01; Dow Corning Corporation: Midland, MI, April 2, 2014.

(23) Callister, W. D.; Rethwisch, D. G. *Materials Science and Engineering: An Introduction*, 8th ed.; John Wiley & Sons, Inc.: Hoboken, NJ, 2010.

(24) *Sylgard® 184 Silicone Elastomer Kit (Base)*; Material Safety Data Sheet No. 802554-00002; Dow Corning: Korea, Nov 29, 2006.

(25) White, M.; Johnson, J.; Koberstein, J. T.; Turro, N. J. Toward the Syntheses of Universal Ligands for Metal Oxide Surfaces : Controlling Surface Functionality through Click Chemistry. *J. Am. Chem. Soc.* **2006**, *128*, 11356–11357.

(26) Garnweitner, G.; Goldenberg, L. M.; Sakhno, O. V.; Antonietti, M.; Niederberger, M.; Stumpe, J. Large-Scale Synthesis of Organophilic Zirconia Nanoparticles and Their Application in Organic-Inorganic Nanocomposites for Efficient Volume Holography. *Small* **2007**, *3*, 1626–1632.

(27) Nishiura, S.; Tanabe, S.; Fujioka, K.; Fujimoto, Y.; Nakatsuka, M. Preparation and Optical Properties of Transparent Ce:YAG Ceramics for High Power White LED. *IOP Conf. Ser. Mater. Sci. Eng.* **2009**, *1*, 012031.

(28) ASTM D5470. Standard Test Method for Thermal Transmission Properties of Thermally Conductive Electrical Insulation Materials; American Society for Testing and Materials: Philadelphia, PA, 2012.

(29) Yavari, F.; Fard, H. R.; Pashayi, K.; Rafiee, M. A.; Zamiri, A.; Yu, Z.; Ozisik, R.; Borca-Tasciuc, T.; Koratkar, N. Enhanced Thermal Conductivity in a Nanostructured Phase Change Composite due to Low Concentration Graphene Additives. *J. Phys. Chem. C* **2011**, *115*, 8753–8758.

(30) Demir, M. M.; Koynov, K.; Akbey, Ü.; Bubeck, C.; Park, I.; Lieberwirth, I.; Wegner, G. Optical Properties of Composites of PMMA and Surface-Modified Zincite Nanoparticles. *Macromolecules* **2007**, *40*, 1089–1100.

(31) *ProLight PR2N-3LxE-SD 3W Power LED*. Technical Datasheet. Version 3.3. Prolight Opto Technology Corporation: Zhongli City, Taiwan, 2014, 1–23.

(32) O'Haver, T. *A Pragmatic Introduction to Signal Processing* [Online]; peakfit.m Matlab Program Version 6.01, October, 2014. https://terpconnect.umd.edu/~toh /spectrum/ (accessed November 1, 2014).

(33) Oh, S. J.; Go, G.; Lee, J.-L.; Schubert, E. F.; Cho, J.; Kim, J. K. Enhanced Phosphor Conversion Efficiency of GaN-Based White Light-Emitting Diodes Having Dichroic-Filtering Contacts. *J. Mater. Chem. C* **2013**, *1*, 5733.

(34) Borilo, L. P.; Spivakova, L. N. Synthesis and Characterization of ZrO_2 Thin Films. *Am. J. Mater. Sci.* **2012,** *2*, 119–124.

(35) Zeni, M.; Hohemberger, J. M.; Bergmann, C. P. Preparation of Crystalline $ZrTiO_4$ at Low Thermal Treatment Temperatures. *Rev. Adv. Mater. Sci.* **2010**, *24*, 44–47.

(36) Sarkar, D.; Mohapatra, D.; Ray, S.; Bhattacharyya, S.; Adak, S.; Mitra, N. Synthesis and Characterization of Sol-Gel Derived ZrO_2 Doped Al_2O_3 Nanopowder. *Ceram. Int.* **2007**, *33*, 1275–1282.

(37) UCT, Inc. Petrarch® Specialty Chemicals: Silanes, Silicones, and Platinum Catalysts. Chromatographic Specialties Inc. Web site. https://www.chromspec.com /pdf/e/uct37.pdf (accessed Jul 1, 2014).

(38) Kobayashi, M.; Matsuno, R.; Otsuka, H.; Takahara, A. Precise Surface Structure Control of Inorganic Solid and Metal Oxide Nanoparticles through Surface-Initiated Radical Polymerization. *Sci. Technol. Adv. Mater.* **2006**, *7*, 617–628.

(39) Keeping, S. Digi-Key Electronics: Royal Blue LEDs : Decoding the Datasheet. http://www.digikey.com/en/articles/techzone/2013/apr/royal-blue-leds-decoding-the-datasheet (accessed June 23, 2014).

(40) Yamamoto, H. White LED phosphors: the next step. *Proceedings of SPIE 7598, Optical Components and Materials VII*, San Francisco, CA, Jan 23, 2010.

(41) Bachmann, V.; Ronda, C.; Meijerink, A. Temperature Quenching of Yellow Ce3+ Luminescence in YAG:Ce. *Chem. Mater.* **2009**, *21*, 2077–2084.

(42) Shuai, Y.; Tran, N. T.; Shi, F. G. Nonmonotonic Phosphor Size Dependence of Luminous Efficacy for Typical White LED Emitters. *IEEE Photonics Technol. Lett.* **2011**, *23*, 552–554.

(43) Tran, N. T.; You, J. P.; Shi, F. G. Effect of Phosphor Particle Size on Luminous Efficacy of Phosphor-Converted White LED. *J. Light. Technol.* **2009**, *27*, 5145–5150.

(44) Pressly, J. Micelles and Nanoparticles: A Novel Approach to Photonic Crystal Synthesis. M.S. Thesis, Rensselaer Polytechnic Institute, Troy, NY, 2014.

(45) Painter, P. C.; Coleman, M. M. *Essentials of Polymer Science and Engineering*; DEStech Publications, Inc.: Lancaster, PA, 2009.

(46) Kumar, A.; Gupta, R. K. *Fundamentals of Polymer Engineering*, 2nd ed.; Marcel Dekker, Inc.: New York, NY, 2003.

(47) Gelest, Inc. Reactive Silicones: Forging New Polymer Links. Gelest Inc.: Literature Web site. http://www.gelest.com/goods/pdf/reactivesilicones.pdf (accessed June 22, 2015).

(48) Ebadi-Dehaghani, H.; Nazempour, M. Thermal Conductivity of Nanoparticles Filled Polymers. In *Smart Nanoparticles Technology* [Online]; Hashim, A., Ed.; InTech, 2012; Chapter 23, pp 519–534. http://www.intechopen.com/books/smart-nanoparticles-technology/thermal-conductivity-of-nanoparticles-filled-polymers- (accessed Feb 7, 2015).

(49) Balachander, N.; Seshadri, I.; Mehta, R. J.; Schadler, L. S.; Borca-Tasciuc, T.; Keblinski, P.; Ramanath, G. Nanowire-Filled Polymer Composites with Ultrahigh Thermal Conductivity. *Appl. Phys. Lett.* **2013**, *102*.

(50) Andriot, M.; Degroot, J. V; Meeks, R.; Gerlach, E.; Jungk, M.; Wolf, a. T.; Cray, S.; Easton, T.; Mountney, A.; Leadley, S.; et al. Silicones in Industrial Applications. In *Inorganic Polymers*; Jaeger, R. D.; Gleria, M., Eds.; Nova Science Publishers: Hauppauge, NY, 2007; pp 61-161.

(51) Deshpande, G.; Rezac, M. E. Kinetic Aspects of the Thermal Degradation of Poly(dimethyl Siloxane) and Poly(dimethyl Diphenyl Siloxane). *Polym. Degrad. Stab.* **2002**, *76*, 17–24.

8. Appendix

Key LED Samples Described

LED Name	Color	Silicone	Phosphor	Phosphor Content [wt%]	Zirconia Content [wt%]
B1_bare	Blue				
(*B1_D10*)	Blue	Sylgard	Dow	10	0
(*B2_S_D10_0*)	Blue	Sylgard	Dow	10	0
(*B4_S_D5_0*)	Blue	Sylgard	Dow	5	0
(*B6_S_D10_0*)	Blue	Sylgard	Dow	10	0
(*B7_S_D5_0*)	Blue	Sylgard	Dow	5	0
(*B10_S_D65_0*)	Blue	Sylgard	Dow	65	0
(*B11_S_D65_0*)	Blue	Sylgard	Dow	65	0
RB12_S_D_0 (*RB12_S_D65_0*)	Royal Blue	Sylgard	Dow	65	0
RB14_MP_O	Royal Blue	Momentive	Osram	65	0
RB17_S_D_33.5 (*RB17_S_D65_33.5*)	Royal Blue	Sylgard	Dow	65	33.5
RB18_S_D_33.5 (*RB18_S_D65_33.5*)	Royal Blue	Sylgard	Dow	65	33.5
RB27_S_O (*RB27_S_O65_0*)	Royal Blue	Sylgard	Osram	65	0
RB29_MP_O	Royal Blue	Momentive	Osram	65	0
RB30_MP_O_33.5	Royal Blue	Momentive	Osram	65	33.5
RB31_MP_O_33.5	Royal Blue	Momentive	Osram	65	33.5
RB32_MP_O_33.5	Royal Blue	Momentive	Osram	65	33.5
RB35_S_O	Royal Blue	Sylgard	Osram	65	0
RB36_S_O_33.5	Royal Blue	Sylgard	Osram	65	33.5
RB39_MP_O	Royal Blue	Momentive	Osram	65	0
RB40_MP_O_33.5	Royal Blue	Momentive	Osram	65	33.5
RB41_MP_O_33.5	Royal Blue	Momentive	Osram	65	33.5

(*label for color space*)	Aging Set 1
Label for all other uses	Aging Set 2